SMC-TC114:

West Coast Wave Initiative Extended Research Program (WCWI-ERP)

WCWI Extended Research Program

Prepared for:

Marine Renewables Canada SMC-TC114

Prepared by:

Dr. B. Robertson, Dr. B. Buckham, Dr. H. Bailey

West Coast Wave Initiative
University of Victoria

Director:
        Dr. Brad Buckham
Project Manager:
        Dr. Bryson Robertson

PO Box 3055 STN CSC
Victoria BC V8W 3P6
Canada

Phone: 250-472-4065
Fax: 250-721-6323

Website: uvic.ca/wcwi
Email: wcwi@uvic.ca

University
of Victoria
Institute for
Integrated
Energy Systems

Table of Contents

1　Introduction

The West Coast Wave Initiative (**WCWI**) Extended Research Program (**ERP**) was completed by the WCWI, a research group within the Institute for Integrated Energy Systems at the University of Victoria. The WCWI is a collaboration of university researchers, international Wave Energy Converter (WEC) developers, and Canadian service providers. The WCWI is mandated to:

1.　develop a highly resolved computational near shore wave propagation model for the west coast of British Columbia
2.　apply this computational model to estimating the gross wave energy resource off of Vancouver Island,
3.　evolve Canadian software for the simulation of floating offshore infrastructure such that it can accurately model Wave Energy Converter (**WEC**) dynamics and calculate the expected WEC power production, and
4.　investigate the mechanisms for integrating WEC supplied power into British Columbia and Western Canada's electrical grids.

Using financial contributions from Marine Renewables Canada (**MRC**), and through new in-kind contributions made by AXYS Technologies, Cascadia Coastal Research Ltd, Nortek USA, Golder Associates, and Sandia National Labs, the WCWI research program was extended to address problems specific to three thematic areas proposed by MRC.　These included:

1.　Wave Resource Modelling and Uncertainty Analysis,
2.　Wave/WEC Interactions and Wave Farm Array Modelling Methodologies, and
3.　Mooring Design and Stress Load Data Collection.

This report details the results and findings of the WCWI Extended Research Program in three major sections as per the three themes provided in the original research (shown in Table 1).

Section 2 Wave Resource Modeling and Uncertainty Analysis focusses on answering questions posed within the MRC Priority Research Areas (**PRA**s) 1.v.1, 1.v.2, 1.iv.1 and 1.iv.2.　As shown in Table 1, WCWI-ERP work included: analysing the uncertainties in computer model based wave resource assessments due to the quality, quantity, and distribution of model boundary conditions; determining uncertainties in wave buoy and AWAC measurements; and uncertainties in gross wave resource assessments due to spectral shape characteristics.

Section 3 Wave/WEC Interactions and Wave Farm Array Methodologies focus on MRC PRA 1.v.3. This work included the development of techniques for including arrays of WEC technologies inside large scale computational near shore wave propagation model.　In the WCWI-ERP, the WCWI existing near shore wave model, built using Simulating WAves Nearshore (SWAN) software, was refined in proposed WEC deployment sites and an algorithm proposed by Sandia National Labs (**SNL**) for including WEC devices in the model was tested.　The tests required building Response Amplitude Operator (**RAO**) curves for individual WEC devices, and implementing these RAOs within the SWAN model.

Section 4 Mooring Design and Load Data Collection focusses on MRC PRA's 1.ii.1 and 1.ii.2. This work included designing and integrating a hermetically sealed load cell on an AXYS TRIAXYS buoy mooring connection to record high resolution mooring loads at the connection point. The mooring load dataset was packaged with sea state data measured by the AXYS TRIAXYS wave buoy itself, an acoustic wave and current (AWAC) profiler and SWAN model outputs to create a unique and comprehensive dataset that can be used to validate mooring dynamics models and evolve knowledge of mooring loads on floating WEC technologies.

Table 1: WCWI-ERP Research Themes. The original proposal identified three distinct thematic areas that each encompassed multiple MRC PRA's. Sections 2, 3 and 4 of the current report present the findings in each theme. Section and page number references are contained to the current report.

WCWI EXTENDED RESEARCH PROGRAM			
Research Themes	**Resource Modelling and Uncertainty Analysis (Section 2)**	**Wave/WEC Interactions and Array Methodology (Section 3)**	**Mooring Design and Load Data Collection (Section 4)**
Associated MRC PRA's	1.v.1 1.iv.1 1.v.2 1.iv.2	1.v.3	1.ii.1 1.ii.2
Objective:	Quantify the major factors affecting wave resource uncertainty and scales of spatial validity of resource data using WCWI SWAN model and wave buoys.	Develop numerical model and methodology to account for WEC interactions and available wave resources within WEC farms.	Acquisition of mooring line load data and platform motion (TRIAXYS buoy platform).
Tasks — Year 1	Task 1.1 (pg. 3): Sensitivity analysis of the wave model spatial validity based on the model wave boundary condition distribution, time frequency and 2D spectrum resolution. Task 1.2 (pg. 13): Deploy collocated TRIAXYS and AWAC at Port Renfrew, BC. Task 1.3 (pg. 15): Determine uncertainty distributions of wave measurement buoy results. Task 1.4 (pg. 16): Utilize 7 years of directional spectral data from WCWI buoys and 10 year SWAN hindcast of wave climate to preform systematic analysis of uncertainties in standardized bivariate distributions due to spectral shape characteristics.	Task 2.1 (pg. 26): Create high resolution SWAN model of possible WEC deployment sites. Task 2.2 (pg. 27): Build normalized frequency domain response curve from WCWI WEC's device simulations. Task 2.3 (pg. 29): Implement demonstration wave array with SWAN model and determine influence on annual wave climate.	Task 3.1 (pg. 33): Design load cell and data acquisition system, install on TRIAXYS mooring line. Task 3.2 (pg. 36): Collect data on buoy motions from accelerometers and rate gyros'. Task 3.3 (pg. 36): During regular buoy maintenance, collect load data during buoy towing, recovery and deployment. Task 3.4 (pg. 36): Compare loads against measured time and frequency domain TRIAXYS and AWAC readings, and frequency domain numerical results from SWAN model.
	Outcome: Detailed understanding of wave resource assessment uncertainties due to boundary conditions, buoy uncertainties and spectral shapes.	**Outcome:** Demonstration of array model, using prospective deployment location and generic WEC curves.	**Outcome:** Extensive dataset of mooring loads under regular operation, deployment and towing.

University of Victoria
Institute for Integrated Energy Systems

2   Resource Modeling and Uncertainty Analysis

In the Resource Modeling and Uncertainty Analysis research, the objectives were to quantify the major factors creating uncertainty in wave resource assessments, and the spatial scales over which resource data generated using the WCWI SWAN model and wave buoys could be extrapolated. The following sections provide detailed information on the methodology and results for Tasks 1.1 through 1.4 listed in Table 1.

2.1   Sensitivity Analysis of the Wave Model Spatial Validity

The sensitivity of the SWAN model outputs to changes in the spatial concentration of boundary conditions (the number and location of the boundary condition data), the boundary condition spectral resolution, and the model's computational time step were studied. For all boundary condition and time step scenarios considered, SWAN data was compared to in-situ wave measurement buoy data. The buoy data is collected from three Environment Canada buoys, two National Buoy Data Centre (NBDC) buoys, as well as three WCWI buoys. Buoy locations are shown in Figure 1 and details provided in Table 2.
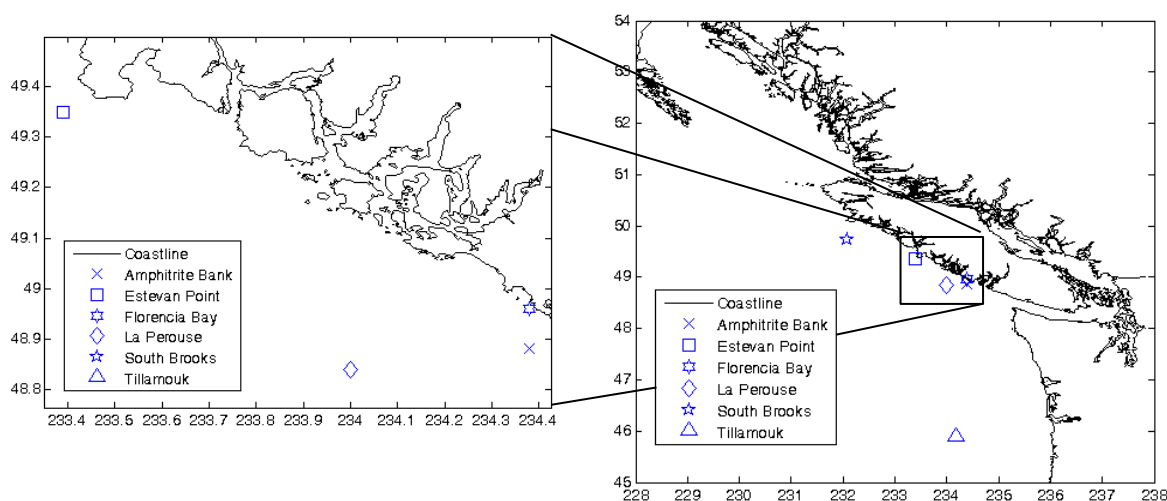
Figure 1: Wave measurement buoy locations

Location	Source	Depth	Starting Date	Resolution	Latitude	Longitude
Amphitrite Bank	WCWI	43 m	4/19/2013	Hourly	48.88 N	125.62 W
Estevan Point	WCWI	42 m	4/23/2013	Hourly	49.35 N	126.61 W
Florencia Bay	WCWI	25 m	6/1/2013	Hourly	48.96 N	125.62 W
La Perouse	EC	73 m	11/22/1988	Hourly	48.84 N	126.00 W
South Brooks	EC	2040 m	5/5/1994	Hourly	49.74 N	127.93 W
Tillamouk	NOAA	2289 m	11/10/2004	Hourly	45.89 N	125.82 W

Table 2: Wave buoy information

The sensitivity analysis was separated into three phases. The first phase investigates the influence of the computational time step; the second phase investigated the influence of the boundary condition spectral resolution; the last phase investigated the influence of the boundary condition spatial resolution. For each scenario, the SWAN model was executed in transient mode for the period January 1st, 2013, 0000 hours to December 31st, 2013, 2300 hours.

The baseline SWAN model inputs are wave boundary conditions at eight stations on the model grid's outer boundary – see Figure 2. At each node, fully directional wave spectra obtained from the European Centre for Medium Range Weather Forecasting (**ECMWF**). The ECMWF wave data features 30 frequency bins, 24 direction bins and 6 hour resolution. Wind forcing over the model spatial domain is

provided by the Coupled Ocean/Atmosphere Mesoscale Prediction System (**COAMPS**) model at three hour resolution. The baseline computational time step used is 3 hours based upon the guidelines set forth in the International Electrotechnical Commission TC 114: Marine energy – wave, tidal and other water current converters draft specification for wave energy resource assessments [1]. For each round of scenarios, the inputs remain constant unless otherwise specified. The baseline state SWAN model set-up is detailed in Table 3 and spatial representation of the boundary modes presented in Figure 3.

Boundary Condition Resolution		Computational Resolution		Computational Time Step	Included Boundary Condition Nodes
Num. Freq.	Num. Dir.	Num. Freq.	Num. Dir.		
30	24	36	36	3 hrs	1 2 3 4 5 6 7 8

Table 3: Baseline SWAN model conditions

Node	Location [deg]
1	46N125W
2	46N 126W
3	47N 127W
4	48N 128W
5	49N 129W
6	50N 130W
7	51N 131W
8	52N 130W
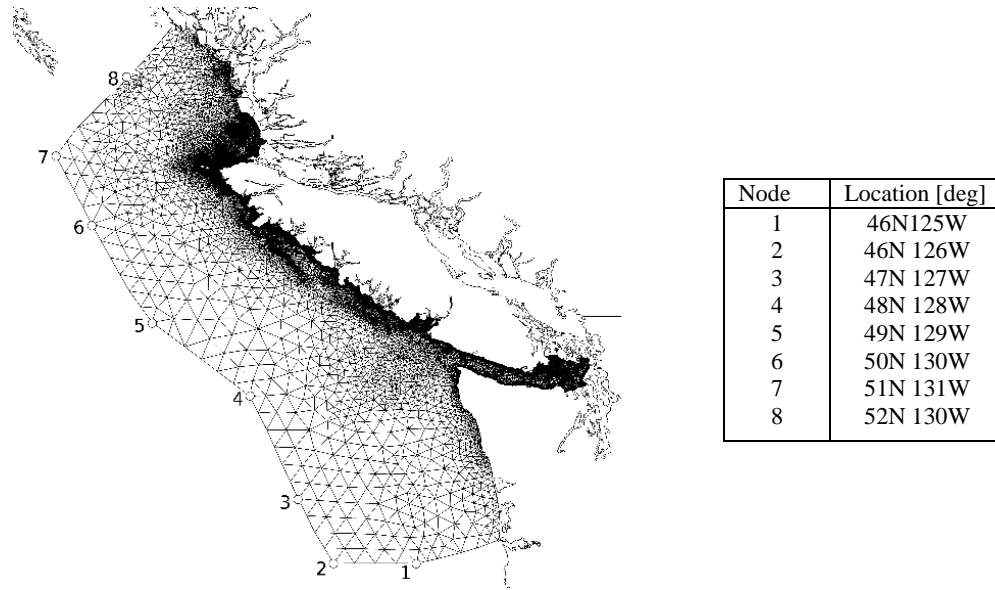
Figure 2: SWAN model boundary condition nodes

In order to compare the SWAN model performance across the scenarios, the following quantitative metrics were calculated: Bias (*B*), root mean square (**RMS**) error (e_{rms}), scatter index (*SI*) and correlation coefficient (*r*). See Eqns. (1) through (4) – note that subscript 'c' indicates the SWAN calculated values, subscript 'm' indicates the buoy measured values and *N* indicates the number of measurements. The bias, RMS error, scatter index and correlation can be applied to any of the statistical wave parameters produced by SWAN and measured by the buoy; in Eqns. (1) through (4), the significant wave height H_s is used simply an example case. For the base case with 3 hour time steps, N = 2920.

$$B = \sum_i \frac{\left(H_{s,c_i} - H_{s,m_i}\right)}{N} \qquad (1)$$

$$SI = \frac{e_{rms}}{\sum_i H_{s,m_i}} \qquad (3)$$

$$e_{rms} = \sqrt{\sum_i \frac{\left(H_{s,c_i} - H_{s,m_i}\right)^2}{N}} \qquad (2)$$

$$r = \frac{N \sum_i \left(H_{s,c_i} H_{s,m_i}\right) - \sum_i H_{s,c_i} \sum_i H_{s,m_i}}{\sqrt{\sum_i H_{s,m_i}}} \qquad (4)$$

B quantifies the average offset magnitude between measured and calculated values, *SI* gives the percentage of expected error for calculated values and *r* indicates the strength and direction of a linear

University of Victoria
Institute for Integrated Energy Systems

relationship between the measurements. Additionally presented below, $\Delta\bar{E}$ presents the mean of the expected value.

2.1.1　First Phase – Varying the Computational Time Step

The schedule of the time step scenarios considered is shown in Table 4. Figure 3 and Figure 4 show the changes in the bias, correlation and scatter index as the computational time step increases. In each of these figures, there are eight measures reported – each value is calculated based on comparison of the SWAN model output with a collocated wave buoy.

Scenario Number	Computational Time Step [hrs]
1A	0.25
1B	0.5
1C	1.0
1D	2.0
1E	3.0
1F	6.0

Table 4: Computational time steps for first round scenario

The following trends are observed as the computational time step is reduced:

- The bias for significant wave height, H_s, at all locations shows an exponential relationship with computational time step.
- In contrast, the bias for peak period, T_P, remains relatively constant as the computational time step increased.
- The correlation for H_s remains relatively constant with only slight decreases as the computational time step transitions from 2 hours to 6 hours.
- The correlation for T_P shows two different trends, one for the WCWI buoy locations and another for the non-WCWI buoy locations. The WCWI buoy locations show a decrease in correlation as the time step is decreased whereas the other locations all remain relatively constant. The exact cause of this difference is still under investigation. However, it is noted that T_P is an unstable parameter and depends on the frequency resolution of the measurement instrument.
- The scatter index showed the same general trends for T_P and H_s as the bias. For H_s, the magnitude of the scatter index decreased as the computational time step was reduced, but the maximum change was 13% at the Neah Bay buoy location. For T_P, the scatter index remained relatively constant without any large variations for all locations.

Table 5 and Table 6 present the relative improvement (positive) or decrease (negative) in the model performance according to the bias, correlation, and scatter index statistics for each SWAN time step at the Tarbotton buoy location. Relative differences are calculated relative to the baseline three hour SWAN time step model.

Scenario Number	1A	1B	1C	1D	1F
$\Delta\bar{E}$	0.81	0.81	0.81	-0.02	0.29
ΔB	64	50	30	27	-43
Δe_{rms}	-1.4	-1.3	-1.3	0.8	-3.1
ΔSI	-2.3	-2.2	-2.1	0.8	-3.4
Δr	-0.37	-0.34	-0.29	0.06	-0.44

Table 5: Relative significant wave height H$_S$ change (%) for the Tarbotton buoy

University of Victoria
Institute for Integrated Energy Systems
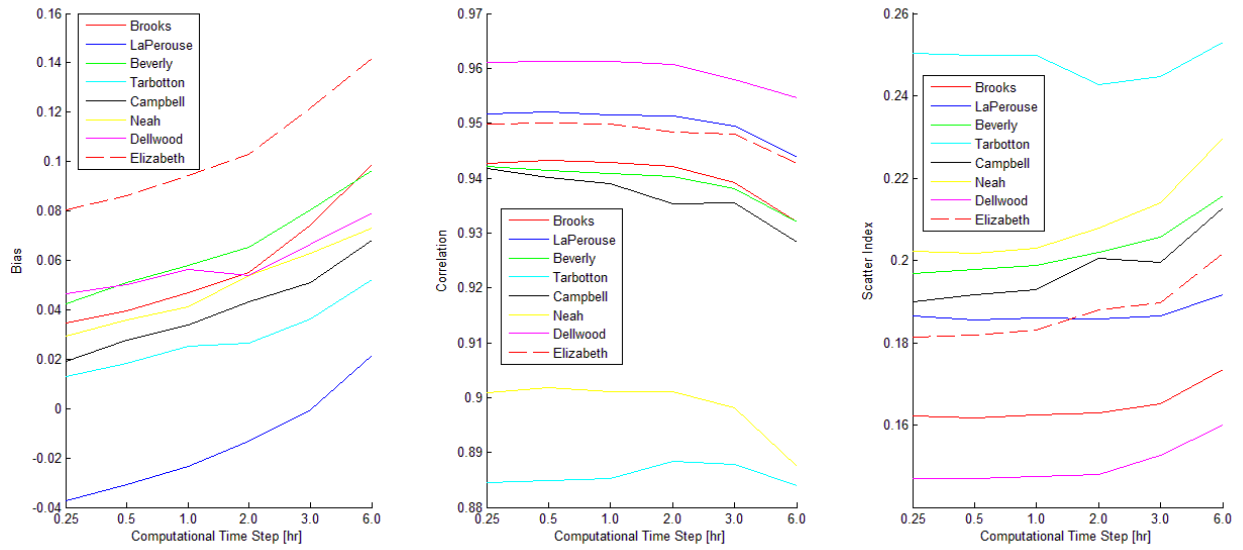
Figure 3: Statistical comparison of significant wave height H_S predictions completed with varying SWAN model time steps
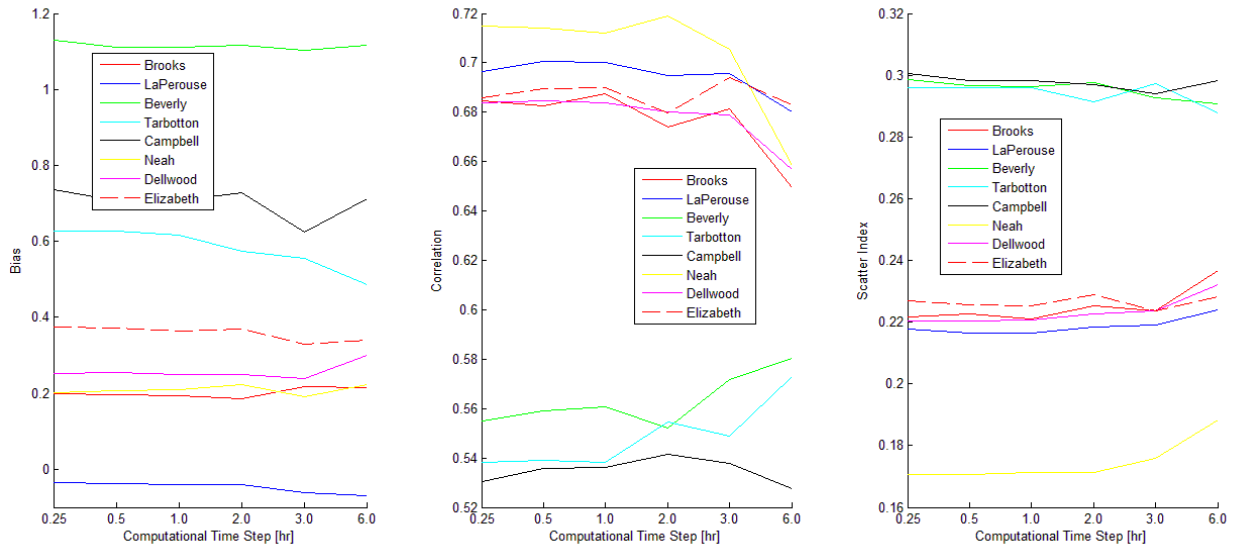
Figure 4: Statistical comparison for peak period T_P predictions with varying SWAN model time steps

Scenario Number	1A	1B	1C	1D	1F
$\Delta \bar{E}$	-0.12	-0.12	-0.12	-0.14	-1
ΔB	-13	-13	-11	-3	13
Δe_{rms}	0.26	0.28	0.27	1.9	2.2
ΔSI	0.37	0.4	0.37	2	3.2
Δr	-1.9	-1.8	-2	1.1	4.4

Table 6: Relative peak wave period T_P statistical change (%) for the Tarbotton buoy

University
of Victoria
Institute for
Integrated
Energy Systems

2.1.2   Second Phase – Varying the Spectral Resolution of the SWAN Boundary Conditions

The spectral resolution of the ECMWF supplied boundary conditions was adjusted by downsampling the original spectrum of 36 direction and 36 frequency bins. Each initial downsampled spectrum was then scaled, according to Eq. (5), to ensure that the zeroth spectral moment (the total variance of the wave spectrum) was preserved in the downsampling process (See Eq. (6)).

$$\text{Correction factor (CF)} = \frac{\iint E_{\text{original}}(f,d)\mathrm{d}f\mathrm{d}\theta}{\iint E_{\text{downsampled, init}}(f,d)\mathrm{d}f\mathrm{d}\theta} \tag{5}$$

$$E_{\text{downsampled, final}} = \text{CF} * E_{\text{downsampled, init}} \tag{6}$$

The downsampled frequency and direction bin center values are shown in Table 8**.** The frequency bins within the boundary conditions are logarithmically spaced within the range 0.035 Hz $\le f \le$ 0.5476 Hz. The direction bins are of uniform width and cover the range $0° \le \theta < 360°$. All 8 BC nodes were used for Phase 2 tests.

It is important to note that the wave boundary condition (BC) resolution does not define the computational resolution used by SWAN. SWAN will interpolate the BC resolution to the user defined computational resolution. For this study, the computational resolution used within SWAN was varied to match the boundary condition resolution. The frequency and direction resolution of both the boundary conditions and the internal SWAN computations are shown in Table 7 for each round of scenarios.

Scenario	Boundary Condition Resolution		SWAN Computational Resolution	
	Num. Freq.	Num. Dir.	Num. Freq.	Num. Dir.
Constant Computational Resolution (Reg Grid)				
2A (Baseline)	30	24	30	30
2B	25	15	30	30
2C	20	10	30	30
2D	15	8	30	30
Consistent Computational Resolution (Low Grid)				
2E	25	15	25	15
2F	20	10	20	10
2G	15	8	15	8

Table 7: Boundary condition and SWAN computational resolution for second round scenario

Figure 4 and Figure 5 present the bias, RMS error, scatter index and correlation coefficient calculated at four of the wave buoy locations; results for only half of the 8 buoy locations are shown to reduce clutter in the figures, and the results for the removed four buoys show similar trends.

Dashed lines indicate the constant computational resolution (reg. grid) cases with lowered boundary condition resolution. The solid lines in the plots represent the consistent computational resolution (low grid) cases where the BC and computational resolution decrease in tandem. Several trends can be seen as the spectral resolution is decreased:

- For significant wave height, H_s, the general trend indicates decreasing model performance as the boundary condition resolution is decreased.
- For peak period, T_P, the model performance remains relatively constant as the boundary condition resolution decreases.

The solid lines show that decreasing the SWAN computational resolution enhances the effects of decreasing the boundary condition resolution.

University
of Victoria
Institute for
Integrated
Energy Systems

Reduced Resolution 1 25 Freq, 15 Dir		Reduced Resolution 2 20 Freq, 10 Dir		Reduced Resolution 3 15 Freq, 8 Dir	
Frequency [Hz]	Direction [degrees]	Frequency [Hz]	Direction [degrees]	Frequency [Hz]	Direction [degrees]
0.0345	-168	0.0345	-162	0.0345	-157.5
0.038712	-144	0.039903	-126	0.042032	-112.5
0.043438	-120	0.046153	-90	0.051208	-67.5
0.048742	-96	0.053382	-54	0.062388	-22.5
0.054692	-72	0.061743	-18	0.076008	22.5
0.06137	-48	0.071413	18	0.092602	67.5
0.068862	-24	0.082598	54	0.112819	112.5
0.077269	0	0.095535	90	0.137449	157.5
0.086703	24	0.110498	126	0.167456	-
0.097288	48	0.127804	162	0.204015	-
0.109166	72	0.147821	-	0.248555	-
0.122494	96	0.170974	-	0.302819	-
0.137449	120	0.197752	-	0.368929	-
0.15423	144	0.228724	-	0.449473	-
0.173059	168	0.264548	-	0.5476	-
0.194188	-	0.305982	-	-	-
0.217896	-	0.353906	-	-	-
0.244498	-	0.409336	-	-	-
0.274348	-	0.473447	-	-	-
0.307843	-	0.5476	-	-	-
0.345427	-	-	-	-	-
0.387599	-	-	-	-	-
0.43492	-	-	-	-	-
0.488019	-	-	-	-	-
0.5476	-	-	-	-	-

Table 8: Reduced boundary condition spectral resolution

Additionally, the relative change in bias, correlation, and scatter index values for the different scenarios are shown in Figure 4 and Figure 5. The results in Table 8 and Table 9 are computed at the Tarbotton buoy location and are relative to the baseline SWAN model configuration detailed in Table 3.

Scenario Number		2B	2C	2D		2E	2F	2G
$\Delta\bar{E}$	Reg. Grid	3.7	4.1	6.9	Low Grid	3	9.2	8.1
ΔB		-43	-99	-110		-76	-95	-220
Δe_{rms}		-0.07	-1.1	-1.8		-0.47	-0.47	-3.2
ΔSI		-0.08	-1.1	-1.6		-0.49	-0.49	-3.2
Δr		0.06	-0.08	-0.11		-0.25	-0.39	-0.87

Table 8: Model relative performance change (%) in significant wave height HS statistics for varying boundary condition and computational resolutions

Scenario Number		2B	2C	2D		2E	2F	2G
$\Delta\bar{E}$	Reg. Grid	8	9.2	8.1	Low Grid	6.6	6.8	5.5
ΔB		-15	-17	-5.4		-41	-64	-49
Δe_{rms}		-0.48	-1.3	-6.6		-4	-5.7	-10
ΔSI		-0.47	-1.4	-6.6		-4	-5.7	-10
Δr		0.78	0.22	-10		-2.7	-3	-12.7

Table 9: Model relative performance change (%) in peak wave period TP statistics for varying boundary condition and computational resolutions
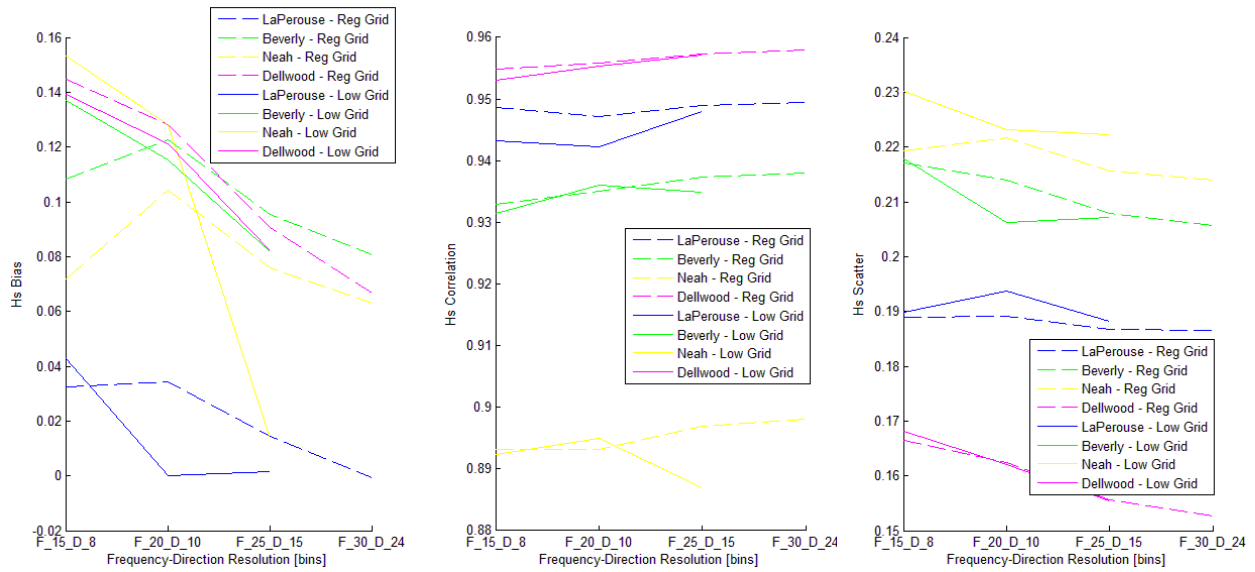
University of Victoria
Institute for
Integrated
Energy Systems

Figure 4: Hs with varying boundary and computational resolutions
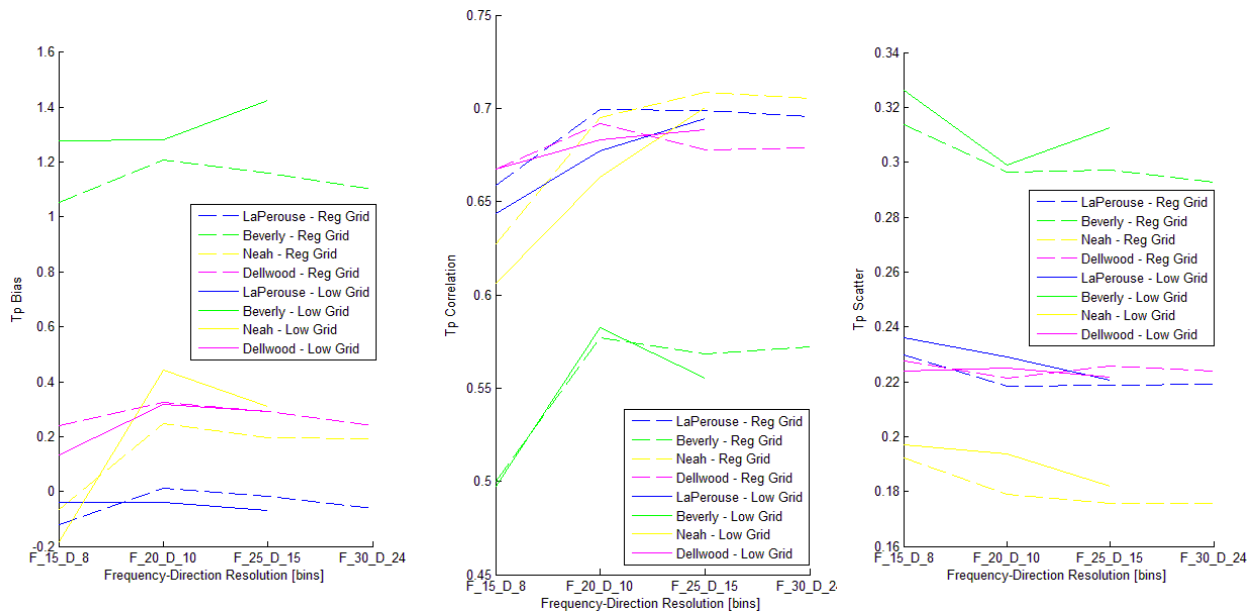

Figure 5: Te with varying boundary and computational resolutions

2.1.3   Third Phase – Varying the Number of Boundary Condition Input Nodes

The third phase of the sensitivity analyses examined the impact of boundary condition spatial positioning and density on the predictions of peak period and significant wave height at the 8 wave buoy sites. The scenarios involved varying both the total number of SWAN model boundary node locations and the locations of these nodes. The baseline system contains eight nodes arranged along the western most boundary of the SWAN computational grid as shown in Figure 2.

A summary of the scenario cases is presented in Table 10 below. For all scenarios, the boundary node numbers refer to the locations shown in Figure 2.

Scenario Number	Boundary Condition Nodes
3A (Baseline)	1 2 3 4 5 6 7 8
3B	1 3 5 7
3C	1 4 8
3D	1 8
3E	1
3F	8
3G	5
3H	4 6
3I	7 3

Table 10: SWAN model boundary node distributions used in Phase 3 of the sensitivity analyses.

Several trends are noted from the results presented in Figure 6 and Figure 7:

- For significant wave height, H_s, decreasing the number of boundary condition locations from 8 to 3 or 4 results in slightly lower correlation and slightly increased scatter index values.
- The largest change in performance occurs when reducing from 3 to 2 boundary condition nodes.
- When using only one boundary condition node, the impacts on performance are very sensitive to the node selection. If node 1 or 8 is utilized, model performance is dramatically decreased (Up to 24% reduction in correlation).
- Table 11 and Table 12 below illustrate the change in bias, RMS error, scatter index and correlation for different boundary scenarios. The reference condition is described in Table 3 and all results are for the Tarbotton buoy.

Scenario Number	3B	3C	3D	3E	3F	3G	3H	3I
$\Delta\bar{E}$	2.4	0.23	6.6	4.5	6	5.3	3.3	3.4
ΔB	-14	100	400	310	370	-150	-55	-64
Δe_{rms}	-0.34	-1	-13	-18	-18	-1.7	0.39	-2.6
ΔSI	-0.37	-1	-13	-18	-18	-1.7	0.37	-2.6
Δr	-0.16	-0.26	-1.6	-4.8	-6.4	-0.53	0.25	-0.63

Table 11: Model relative performance change (%) in significant wave height H$_S$ statistics for varying distribution and density of boundary conditions

Scenario Number	3B	3C	3D	3E	3F	3G	3H	3I
$\Delta\bar{E}$	4.7	2.8	0.63	5.2	1.6	4.4	5.3	4.3
ΔB	23	55	97	11	133	24	11	29
Δe_{rms}	0.49	0.11	0.62	-1.8	-3.3	-0.18	0.42	0.88
ΔSI	0.47	0.1	0.61	-1.9	-3.3	-0.2	0.4	0.87
Δr	-1.5	-3.7	-4.7	0	-9.8	-3.5	-0.86	-3.4

Table 12: Model relative performance change (%) in peak wave period T$_P$ statistics for varying distribution and density of boundary conditions
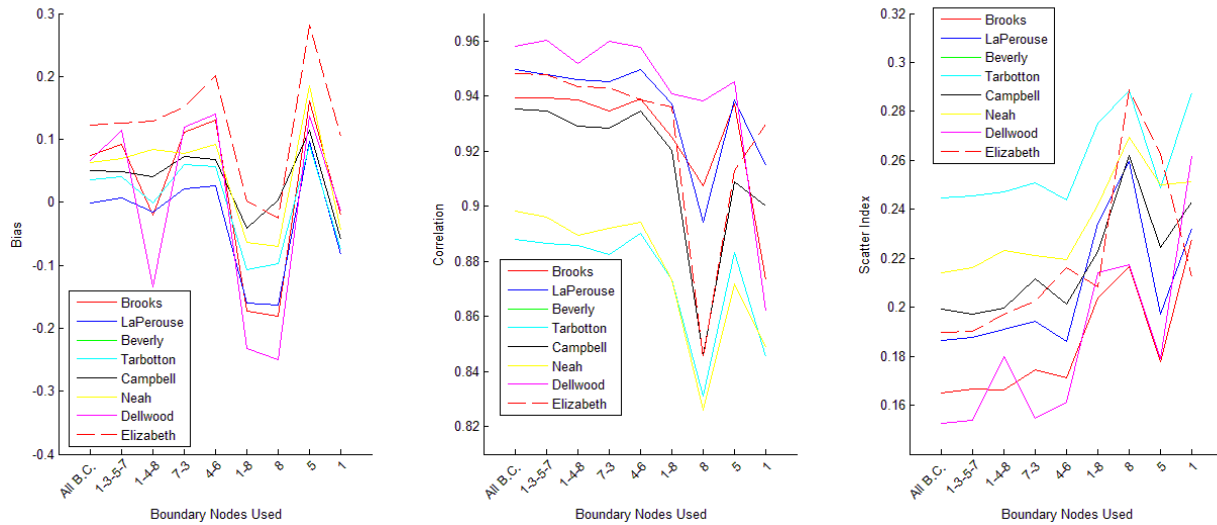
Figure 6: Statistical comparison for significant wave height HS with varying distribution and density of boundary condition nodes
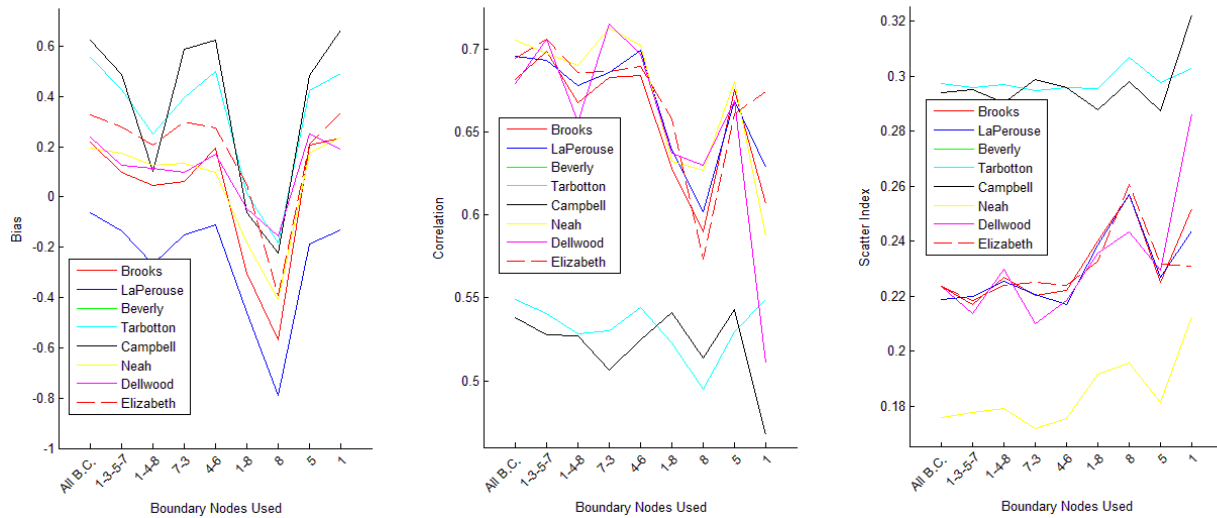
Figure 7: Statistical comparison for peak wave period TP with varying distribution and density of boundary condition nodes

2.1.4 Sensitivity Analysis Conclusions and Recommendations

In wave model spatial validity sensitivity analysis, three major factors affecting the model performance were analyzed; computational time steps, boundary condition resolution, and boundary condition spatial distribution.

The bias for significant wave height, H_s, indicates an exponential relationship with computational time step, while the correlation remains relatively constant with only slight decreases as the computational time step transitions from 2 hours to 6 hours. Similar trends were noted for scatter index measures. As expected, the increased computational time step increased model predictability but also greatly increased the computational expense. It is suggested that a 2 – 3 hour computational time step presents a good compromise of computational efficiency and model performance.

As expected, reductions in boundary condition spectral resolution had negative effects on significant wave height predictions. Negligible effects were noted with regards to peak period. This highlights the unstable nature of the peak period and confirms the need to use energy period for these sorts of comparisons. This work continues within WCWI. However, given that boundary condition spectral resolution has marginal effects on the model computational speed, it is recommended that highest possible spectral resolution is used for resource assessments.

Reductions in the number of boundary condition locations, from 8 to 3 or 4, results in only slightly lower correlation and slightly increased scatter index values for the significant wave height. The most significant change occurs when reducing from 3 to 2 boundary condition nodes. Given that 2 of the boundary condition nodes are located on the lateral model boundaries, and sufficiently distant from the validation buoys, these nodes are assumed to have negligible effect on the model performance. Of the remaining 6 nodes, 3 nodes may still provide sufficient model performance. This equates to a maximum recommended boundary conditions spatial distribution of 200 km/node.

2.2   Wave Measurement Buoy Uncertainties

The sensitivity analyses of Section 2.1 are executed using wave measurement buoy data as reference signals. However, measurement of wave heights and frequencies is itself subject to uncertainties that arise in the conversion of buoy motion data into measures of the wave profiles. To quantify these measurement uncertainties, a new AXYS TRIAXYS wave measurement buoy was collocated with a Nortek Acoustic Wave and Current (**AWAC**) profiler in the southern extent of the SWAN model shown in Figure 2. In this section, the methods for TRIAXYS and AWAC profiler data collection and analysis are summarized. The TRIAXYS wave measurement buoy will be revisited in Section 4, which presents the results of mooring line load data collection completed using a load cell integrated into the Renfrew buoy's data acquisition system.

2.2.1   Deployment of the Collocated Renfrew buoy and AWAC

An AXYS TRIAXYS wave measurement buoy, hereafter referred to as the "Renfrew" buoy, and the AWAC profiler were collocated at the south-western entrance to Port San Juan, located off of the township of Port Renfrew, at coordinates 48°32.187'N 124°29.220'W. The TriAxys buoy outputs wave direction in discrete 3° segments (121 bins) and periods between 1.5 and 33 s. The AWAC outputs wave direction in discrete 2° segments (180 bins) and periods between 1.0 and 50 s. The Renfrew buoy and AWAC deployment locations are detailed in Figure 8.
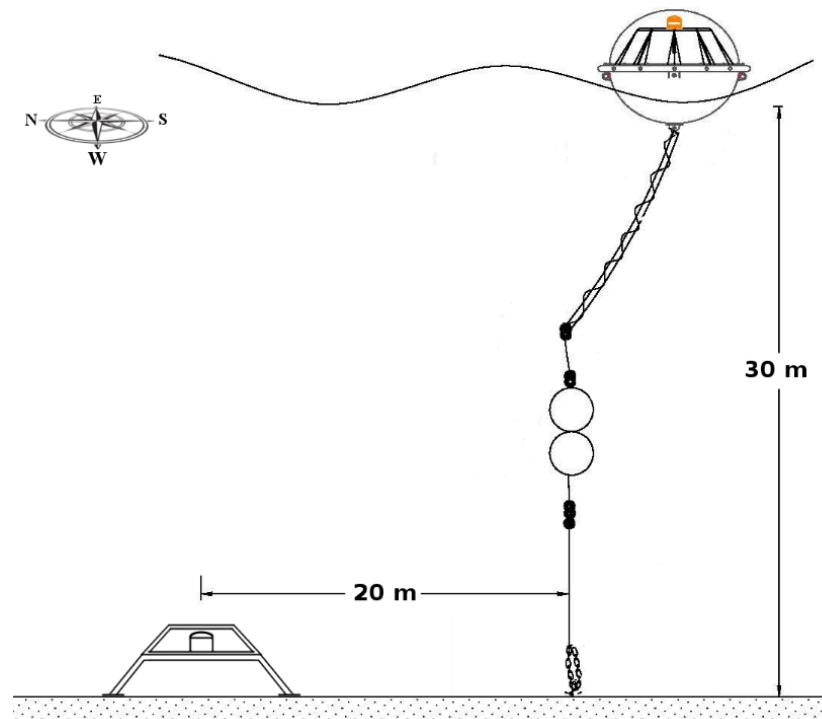
Figure 8: The location of the new TRIAXYS buoy and the Acoustic Wave and Current (AWAC) Profiler.

The devices were deployed on September 26th, 2014 at mean ocean depth of 30 m. The 30 m depth was required since the AWAC, donated to the project by Nortek Instruments, had a maximum operating depth of 50 m. Additionally, given the risk of equipment loss during a self-contained seafloor deployment, 30 m was determined to be suitable for diver recovery if needed. To maintain correlation between the devices but to avoid direct measurement interference with the buoy mooring line, the AWAC was situated approximately 20 m north from the TRIAXYS buoy.

The AWAC was outfitted with a self-contained power unit that is able to provide power for approximately four months. For this reason, the AWAC and its data was recovered on January 8, 2015 and returned to Nortek. The AWAC mount was on short-term loan from Golder Associates and was returned after recovery. The TRIAXYS buoy remains at its deployed location and continues to operate for public safety and as a shallow water WCWI SWAN model validation point. The following photographs were taken during the buoy and AWAC deployment.
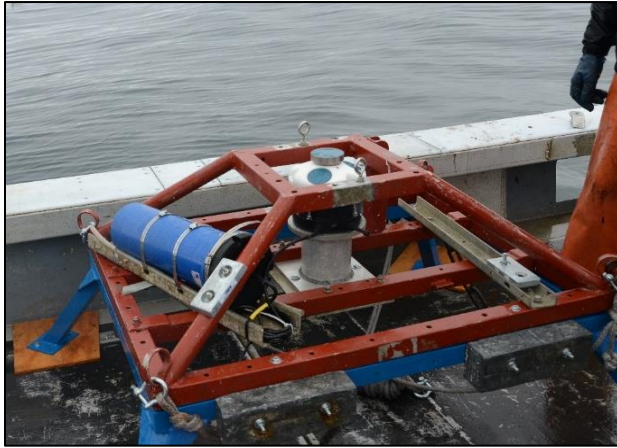
Figure 9: **Acoustic Wave and Current Profiler (AWAC) prior to its deployment**

Figure 10: Lowering the AWAC to the seafloor

Figure 11: TRIAXYS buoy being transported to the measurement site in Port Renfrew

Figure 12: TRIAXYS buoy deployed

2.2.2 Data Analysis (Calculating Wave Buoy Uncertainties)

Detailed uncertainty analysis followed the 'First 5' methodology approach used by the Joint WMO-IOC Technical Commission for Oceanography and Marine Meteorology (**JCOMM**). This methodology was designed to allow for direct comparison of differing wave measurement devices. In the current work, the 'First 5' calculations were implemented using the Wave Evaluation Tool (**WET**) inter-comparison program that is provided freely by JCOMM [2].

The WET utilizes the first five Fourier coefficients, calculated from the directional wave spectrums, from two measurement devices. The directional distribution in each non-directional frequency bin can be described by using Fourier coefficients [3]:

$$E(f,\theta) = \frac{1}{2}a_0 + a_1 \cos\theta + b_1 \cos\theta + a_2 \cos 2\theta + b_2 \sin 2\theta + a_3 \cos 3\theta + b_3 \sin 3\theta \cdots \qquad (7)$$

where $E(f,\theta)$ is directional spectral density for a specific frequency and a_0, a_1, a_2, b_2, a_3, b_3 are the Fourier coefficients per frequency. The above equation is truncated to the first five terms. The coefficients of these terms can be determined by using the following equations:

$$a_0 = \frac{1}{\pi}\int_0^{2\pi} E(f,\theta)d\theta \qquad (8)$$

$$a_1 = \frac{1}{\pi}\int_0^{2\pi} E(f,\theta)\cos\theta\, d\theta \qquad (9) \qquad\qquad b_1 = \frac{1}{\pi}\int_0^{2\pi} E(f,\theta)\sin\theta\, d\theta \qquad (11)$$

$$a_2 = \frac{1}{\pi}\int_0^{2\pi} E(f,\theta)\cos 2\theta\, d\theta \qquad (10) \qquad\qquad b_2 = \frac{1}{\pi}\int_0^{2\pi} E(f,\theta)\sin 2\theta\, d\theta \qquad (12)$$
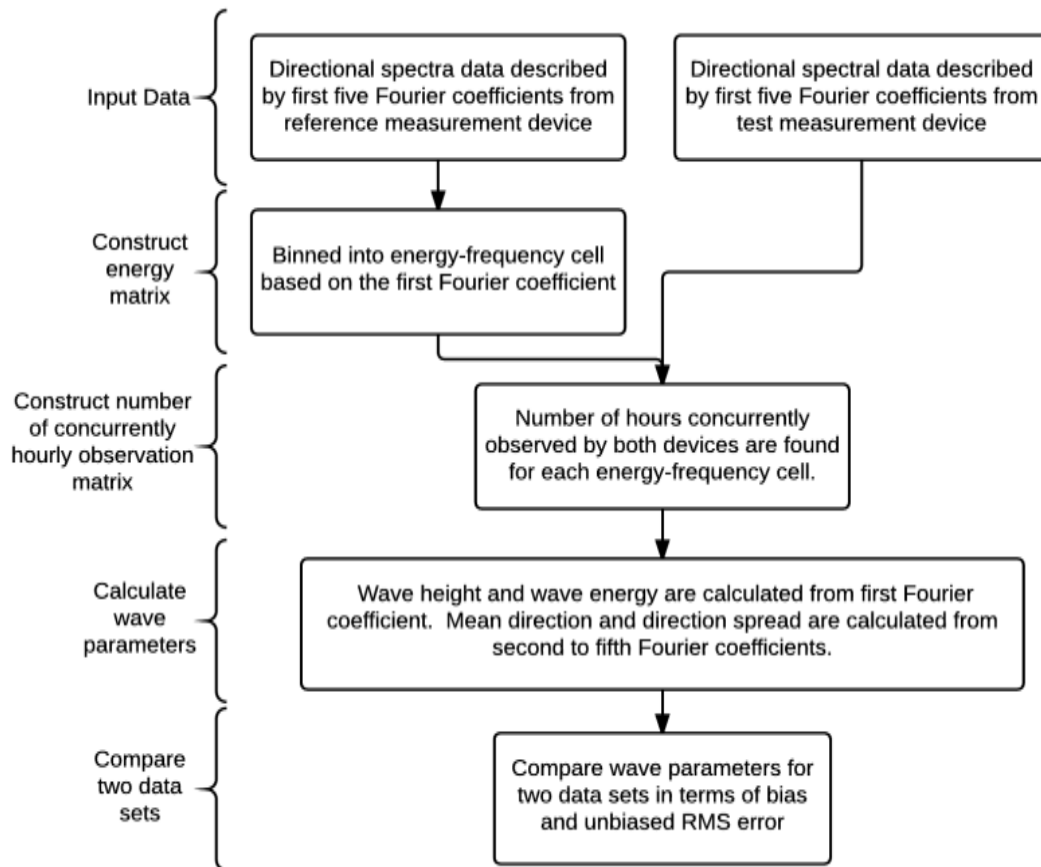
Figure 13: WET flow chart

Initially, the WET program constructs a matrix comprised of 17 energy rows and 48 frequency columns. The energy values in the matrix are calculated by multiplying the spectral density (i.e. first Fourier coefficient) by the frequency respective bandwidth. The number of concurrent observational hours, from both devices, is then determined and plotted in the energy matrix (Figure 14). The bias and RMSE, between the reference and test device, is then calculated for the significant wave height, spectral energy, wave direction and directional spread respectively. These results provide a quantitative measure of the measurement uncertainty between the two measuring devices as a function of both energy level and frequency. A computational flow chart for the WET program is shown in the Figure 13 above. Interested readers are directed to [4] [5] for further information

For this study, the AWAC was considered as the reference data source [6]. The concurrent buoy and AWAC dataset runs from September 26th, 2014, 0900 hours to January 7th, 2015, 0400 hours.

2.2.3   First 5 Comparison Results

The concurrent hourly observation plot shown in Figure 14 indicates the number of hours the Renfrew buoy collected wave data, according to the energy-frequency bins associated with AWAC (reference device) measurements. The majority of concurrent hourly observations were recorded in the frequency range between 0.07 Hz to 0.3 Hz. Within the 0.07 Hz to 0.3 Hz band, observations at low wave frequencies were concentrated at high energy levels while most of the observations for high frequency waves were concentrated in low energy regions. This is due to the inherent process of wave generation and the limit of wave steepness prior to breaking (additionally plotted in Figure 14).

As results are presented in forthcoming sections, it should be noted that the comparative results in certain energy-frequency bins may be effected by smaller than ideal concurrent observations. In order to mitigate some of these effects, all bins with < 10 concurrent observations were omitted from further investigation.
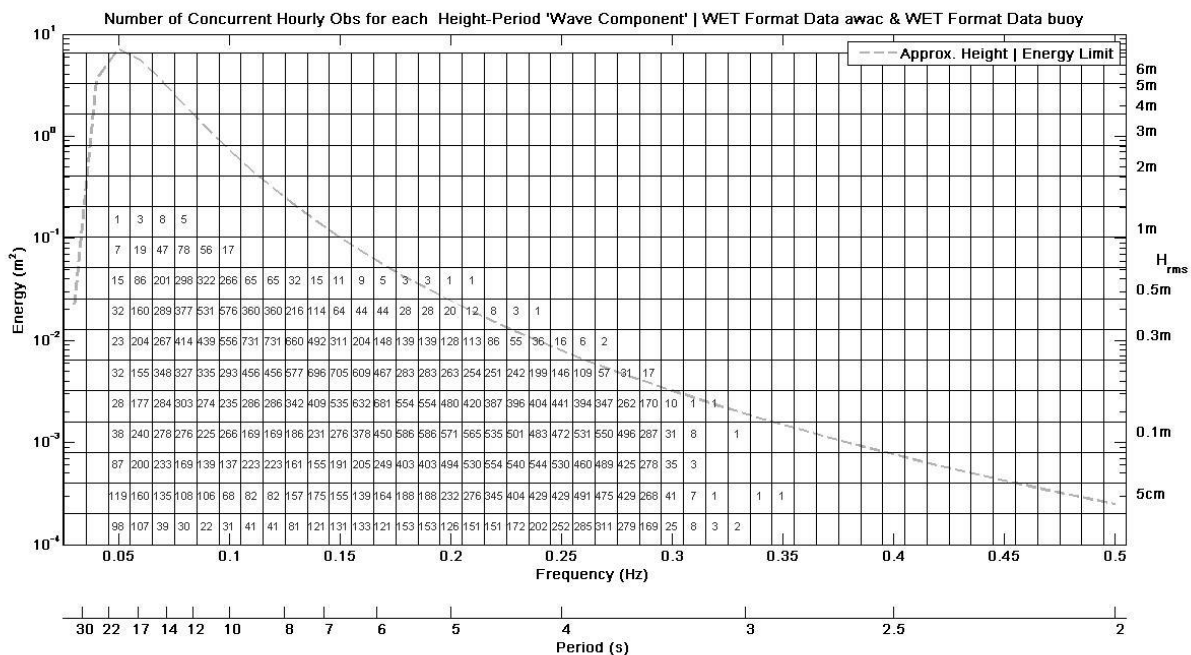
Figure 14: Number of concurrently hourly observations between the AWAC and buoy.

Significant Wave Height Plot

Overall, the measured significant wave height measurements between the AWAC and buoy were consistent. The most significant agreement occurs in the middle to high energy range (between 10^{-3} m^2 and 10^{-1} m^2) with absolute bias values between 0% and 5%. At large significant wave heights, positive bias values indicate that the TRIAXYS buoy generally reports larger significant wave heights the AWAC. The bias decreases and becomes negative values as the energy/significant wave height decreases. There is significant disagreement between the two devices at low energy and low frequency ranges. This can be explained by the low signal to noise ratio in both measurements, and the reduced number of concurrent observations. Generally, the unbiased RMSE increases as frequency and energy decreases. In all subsequent figures, light blue colour is used to represent low values, while red is used for high values.

Figure 15: Average significant mean height bias.

Figure 16: Wave height unbiased RMSE

Spectral Energy Plot

In general, the energy values follow similar trends found in the significant wave height plot; wave energy is under predicted by the wave buoy in low energy situations and over predicted in the most energetic sea states. The increased bias and unbiased RMSE value results from the proportionality of energy to the square of the wave height.
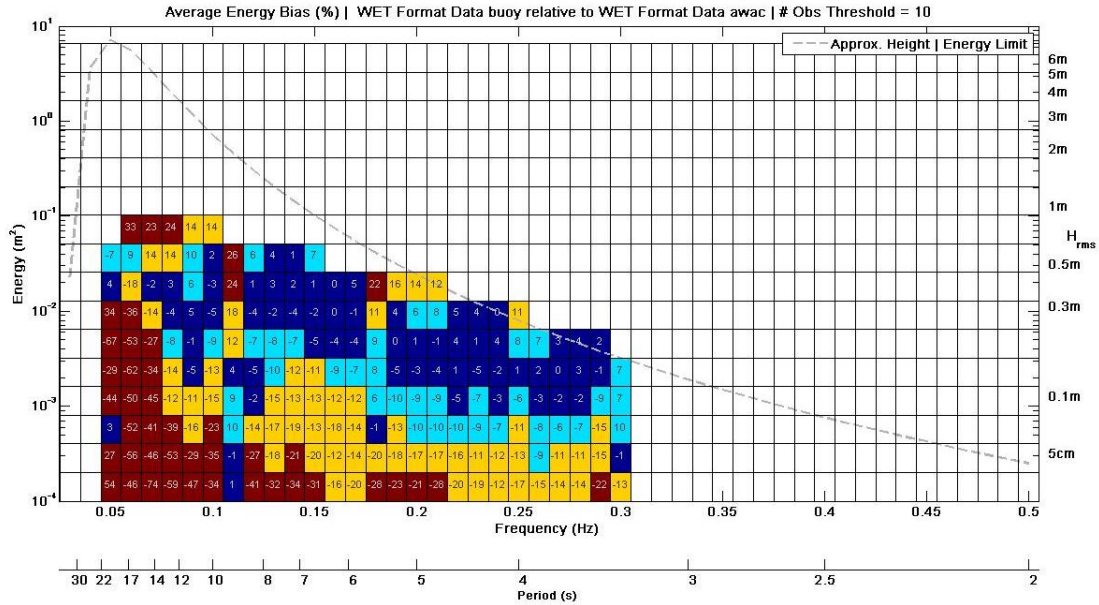
Figure 17: Average wave energy bias
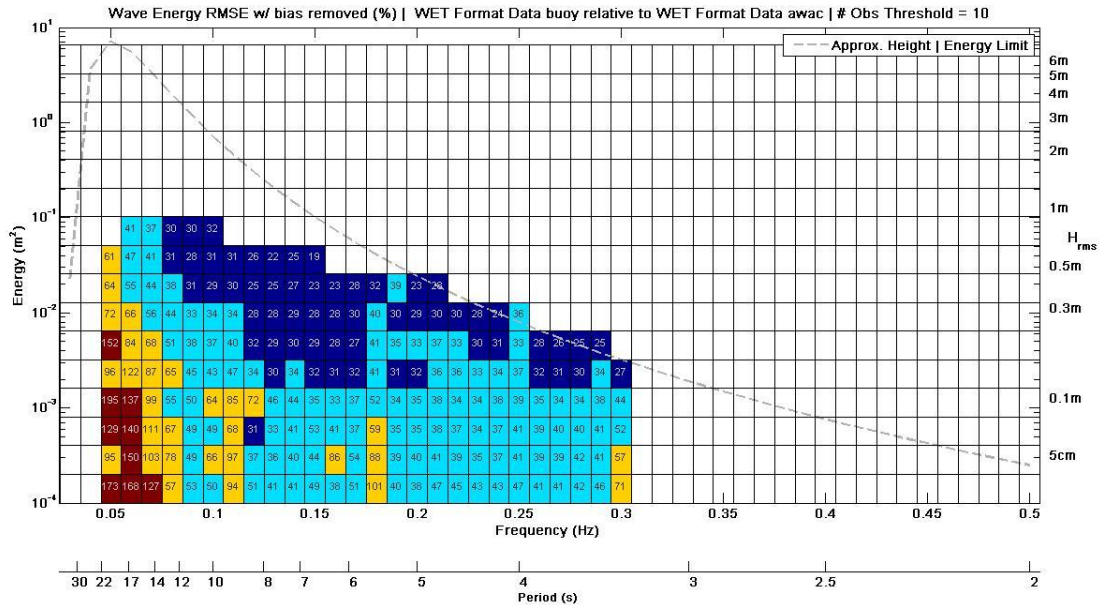
Figure 18: Wave energy unbiased RMSE

Mean Direction Plot

The mean directional bias between the AWAC and buoy are commonly consistent. Slightly higher bias values were found in the low energy scenarios. These outliers are due to low signal to noise ratios at low energy ranges and low concurrent observation hours. The unbiased RMSE plot shows the low RMSE values between the AWAC and buoy in high energy sea states, which feature larger significant wave heights, and the high RMSE values in low energy sea states.
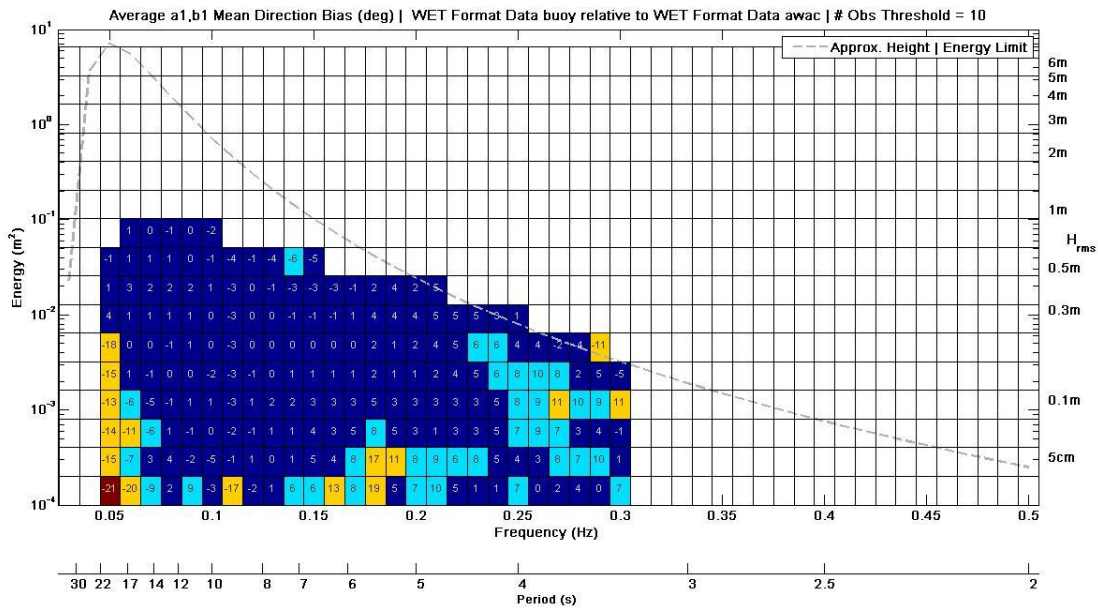
Figure 19: Average mean direction bias based on the second and third Fourier coefficient
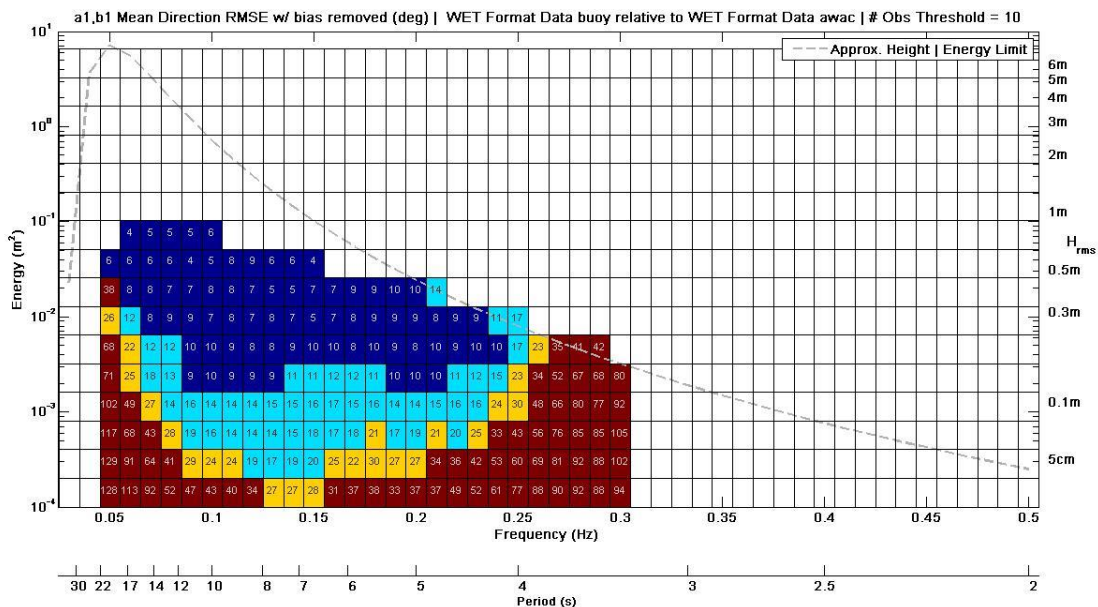
Figure 20: Mean direction unbiased RMSE on the second and third Fourier coefficient

Directional Spread Plot

The directional spread plot shows small bias values at frequency ranges below 0.1 Hz, independent of wave height. These low frequency waves are typically more developed and have lower directional spreading values. As expected, higher biases occur at high frequency regions. The unbiased RMSE for directional spread is small for the entire frequency and energy region.
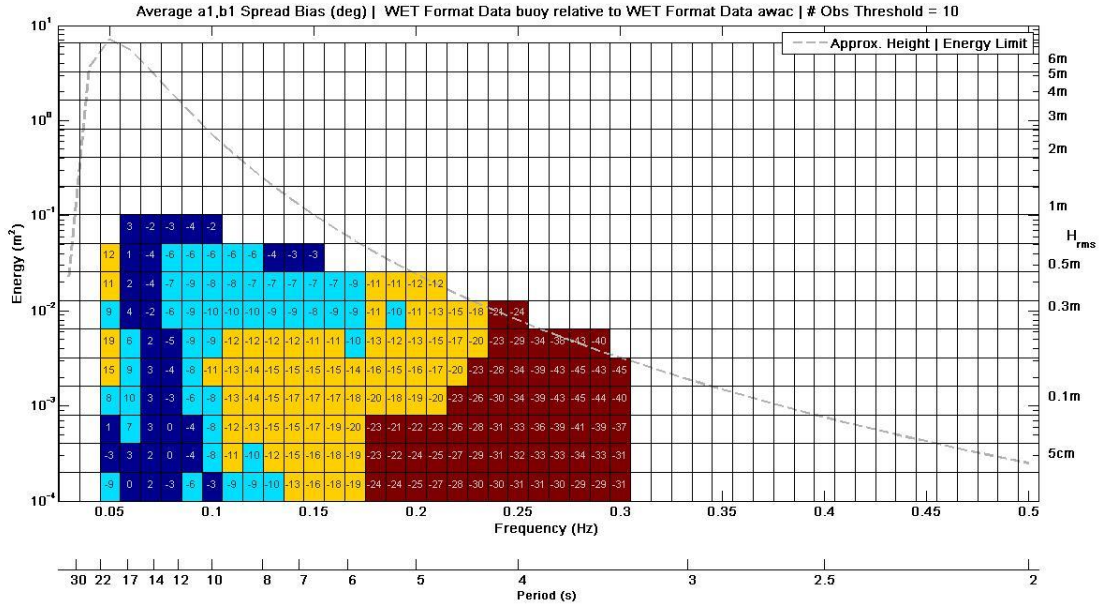
Figure 21: Average directional spread bias based on the second Fourier coefficient
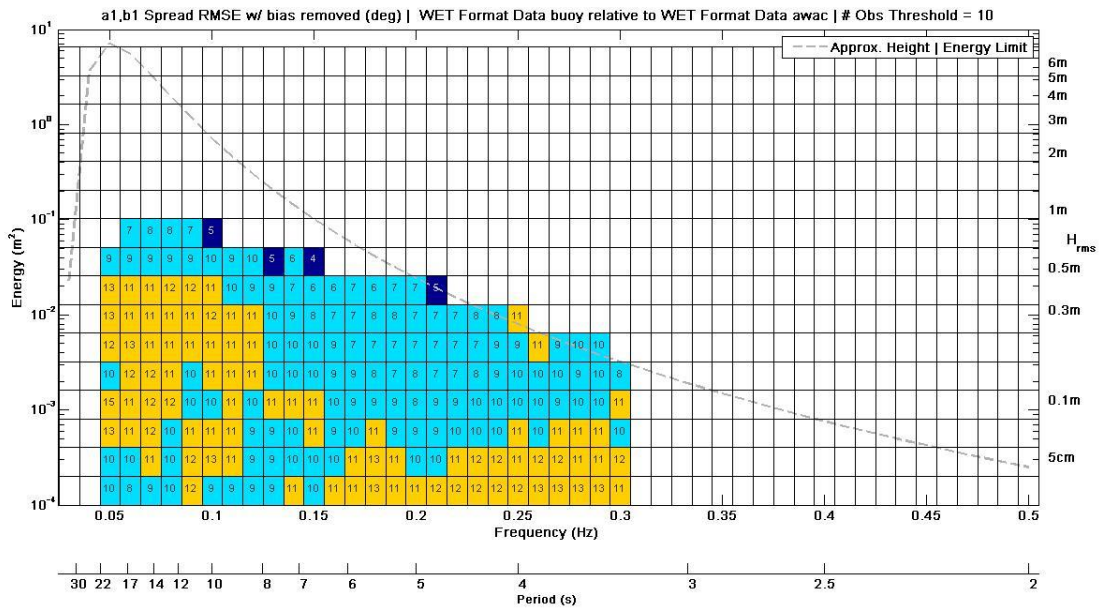
Figure 22: Directional spread of unbiased RMSE on the second and third Fourier coefficient

2.2.4   Measurement Device Uncertainty Conclusions and Recommendations

Port Renfrew, British Columbia, served as an excellent location to test wave measurement buoy uncertainties due to the ease of access, the local wave climate and access to marine infrastructure.

Using the JCOMM 'First 5' Analysis, the wave measurement buoy and AWAC were shown to record consistent significant wave height measurements. Assuming the AWAC measurements were more accurate, the bias and RMSE error associated with the wave measurement buoy increased in low frequency and low energy seastates. This effect is further emphasized in the associated energy plots due to the exponential dependence of wave energy transport on the significant wave height, with a maximum of 74 % underestimation of energy in a single bin.

Directionally, the buoy featured very little relative bias yet the RMSE error was shown to be dependent on the wave frequency. At the high and low frequency extremes, the buoy suffered from significant RMSE. Finally, the TriAxys buoy underrepresents the directional spread of high frequency seastates (> 0.17 Hz).

Given the minimal interest in generating wave power in very low or high frequency seastates, the effect of the noted uncertainties may be minimal. Additionally, it is noted that this study would have benefitted from a longer device deployment and the associated increased occurrence of all seastates. Some of the noted effects may be attributed to limited concurrent measurement occurrences.

2.3   Uncertainties in Standardized Bivariate Histogram

The TC-114 Technical Specification [1] recommends using a bivariate histogram, showing annual hours of occurrence parameterized by significant wave height of 0.5 m bins and wave energy period of 1 s bins, to quantify and assess the gross wave resource. An example histogram for the Campbell buoy is shown in Table 13.

<div align="center">Wave Energy Period (s)</div>

	3.5	4.5	5.5	6.5	7.5	8.5	9.5	10.5	11.5	12.5	13.5	14.5	15.5	16.5	17.5	18.5	Total
0.25	0	0	0	0	0	1	8	5	0	0	0	0	0	0	0	0	14
0.75	0	7	63	189	298	267	247	120	40	4	1	0	0	0	0	0	1236
1.25	0	4	145	508	665	476	338	164	85	15	5	7	2	0	1	0	2415
1.75	0	0	27	213	379	407	232	139	102	46	12	12	0	0	2	0	1571
2.25	0	0	0	73	190	291	362	231	115	50	18	3	3	1	0	0	1337
2.75	0	0	0	15	82	160	193	146	104	62	19	3	6	3	1	0	794
3.25	0	0	0	2	40	102	154	81	58	49	17	6	6	4	0	0	519
3.75	0	0	0	0	4	46	81	56	36	17	13	4	3	2	1	2	265
4.25	0	0	0	0	1	23	48	36	38	13	8	4	1	0	1	0	173
4.75	0	0	0	0	0	6	28	27	24	11	3	0	0	2	2	0	103
5.25	0	0	0	0	0	0	6	17	5	5	3	1	0	1	0	0	38
5.75	0	0	0	0	0	0	3	8	8	6	12	1	0	1	0	0	39
6.25	0	0	0	0	0	0	0	3	0	3	2	3	0	0	0	0	11
6.75	0	0	0	0	0	0	0	1	0	1	2	3	2	0	0	0	9
7.25	0	0	0	0	0	0	0	1	1	1	0	0	0	0	0	0	3
7.75	0	0	0	0	0	0	0	0	0	0	0	0	0	0	0	0	0
Total	0	11	235	1000	1659	1779	1700	1035	616	283	115	47	23	14	8	2	

Wave Height (m)

<div align="center">**Table 13: Bivariate histogram for the Campbell buoy during 2013**</div>

University of Victoria
Institute for Integrated Energy Systems

The standard bivariate histogram provides no detail on the representative spectral shapes for each bin within the histogram. Generally, a JONSWAP or Pierson-Moskowitz (PM) spectrum is assumed. This assumption introduces significant uncertainties between the resulting synthesized spectrum, based on assumed spectral shape, and the actual buoy measured spectrum. As shown in Figure 23, the measured and assumed variance density distributions can vary significantly.
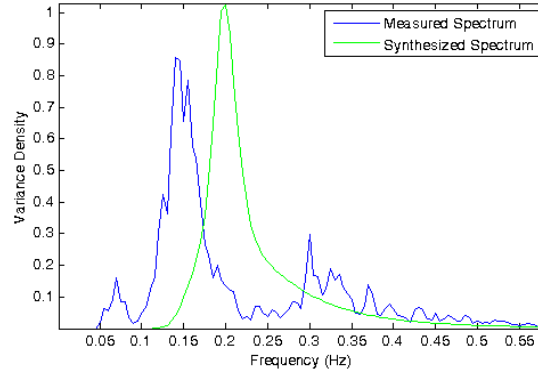
Figure 23: Example measured wave spectrum and representative JONSWAP spectrum

In order to better quantify the best-fit spectral shape for each histogram bin, the wave spectrums from the four WCWI buoys were binned according to the appropriate histogram significant wave heights and energy periods. An aggregate wave spectrum for each bin was then created by averaging all the spectrums in the individual bins. A best fit JONSWAP spectrum was found for each aggregate spectrum by varying γ, the JONSWAP peak-enhancement factor, in Eq. (13) between 1 and 7, in 0.1 increments, until the relative difference between the measured spectrum and synthesised spectrum is minimized. The equation used to describe JONSWAP utilizes α, the energy scale, and σ, the spectral peak width.

$$E(f) = \alpha g^2 (2\pi)^{-4} f^{-5} \exp\left[-\frac{5}{4}\left(\frac{f}{f_{\text{peak}}}\right)^{-4}\right] \gamma^{\exp\left[-\frac{1}{2}\left(\frac{f/f_{\text{peak}}-1}{\sigma}\right)^2\right]} \tag{13}$$

where the peak width parameters, σ_a and σ_a, are kept constant at 0.07 and 0.09 respectively. α is calculated so that $\int S(w)\,dw = H_{mo}^2/16$ [Brodtkorb *et al.*, 2000]. In order to quantify the relative difference between measured spectrum and synthesised spectrum, RMS Relative Error (ER) [7] was used in Eq. (14):

$$\text{ER} = 100\sqrt{\sum_{i=1}^{n}(H_{\text{bc}} - H_{\text{bm}})^2 / \sum_{i=1}^{n} H_{\text{bm}}^2} \tag{14}$$

where H_{bc} and H_{bm} are the calculated and measured wave heights respectively. The tables below illustrate the distribution of γ values and associated ER values for each histogram bin for the four WCWI buoys. Research from Robertson *et al.* [8] provides more details on the procedure.

Some general trends can be extrapolated from the tables below:

- A γ value of 1 (representing a PM spectrum) provides the most consistent agreement with the measured spectrums.
- Increased γ values occur for increased wave energy periods.
- Low and high significant wave heights generally result in increased γ values.

University of Victoria
Institute for
Integrated
Energy Systems

		Wave Energy Period (Te)																		
		0.5	1.5	2.5	3.5	4.5	5.5	6.5	7.5	8.5	9.5	10.5	11.5	12.5	13.5	14.5	15.5	16.5	17.5	18.5	19.5
Wave Height (Hmo)	0.25	0	0	0	0	0	0	0	2.8	1.1	1.1	1.1	4.6	0	0	0	0	0	0	0	0
	0.75	0	0	0	0	0	2.5	1	1	1	1	1	1	1.6	1.8	2.3	3.2	6.4	0	0	0
	1.25	0	0	0	0	0	1.6	1	1	1	1	1	1	1	1.3	2.6	2.5	1.6	1.6	3	1
	1.75	0	0	0	0	0	0	1.1	1	1	1	1	1	1	1	1.4	2.6	0	0	0	0
	2.25	0	0	0	0	0	0	1.1	1.1	1	1	1	1	1.2	1.1	1.4	1	4	0	0	0
	2.75	0	0	0	0	0	0	0	1.2	1	1	1	1.2	1.1	1.4	1.7	2.5	2.1	4.1	0	0
	3.25	0	0	0	0	0	0	0	1.8	1	1	1	1.2	1.2	1.3	2.9	4.1	4	3.4	0	0
	3.75	0	0	0	0	0	0	0	3.4	1.2	1.1	1	1.2	1.2	2.2	0	3	4.7	6	0	0
	4.25	0	0	0	0	0	0	0	0	2	1.4	1	1	1.2	1.2	0	0	0	0	0	0
	4.75	0	0	0	0	0	0	0	0	1.8	1.2	1.5	1.1	2.2	1.6	0	0	0	0	0	0
	5.25	0	0	0	0	0	0	0	0	4.3	2.1	1.3	1	1.1	2.2	3.6	0	0	0	0	0
	5.75	0	0	0	0	0	0	0	0	0	1	1.9	0	1	0	2.3	0	0	0	0	0
	6.25	0	0	0	0	0	0	0	0	0	2.2	1	0	1	0	2.5	0	0	0	0	0
	6.75	0	0	0	0	0	0	0	0	1.4	0	0	0	0	0	0	0	0	0	0	0

Table 14: Gamma values for representative spectrum (Campbell Buoy)

		Wave Energy Period (Te)																			
		0.5	1.5	2.5	3.5	4.5	5.5	6.5	7.5	8.5	9.5	10.5	11.5	12.5	13.5	14.5	15.5	16.5	17.5	18.5	19.5
Wave Height (Hmo)	0.25	0	0	0	0	0	0	0	64	68	64	68	63	0	0	0	0	0	0	0	0
	0.75	0	0	0	0	0	34	32	38	94	66	49	31	20	25	21	40	25	0	0	0
	1.25	0	0	0	0	0	45	29	37	62	114	79	39	27	33	28	39	66	65	31	58
	1.75	0	0	0	0	0	0	20	24	35	32	33	27	26	44	53	40	0	0	0	0
	2.25	0	0	0	0	0	0	27	22	28	21	28	19	15	20	33	84	40	0	0	0
	2.75	0	0	0	0	0	0	0	21	20	13	18	18	14	23	25	41	31	50	0	0
	3.25	0	0	0	0	0	0	0	17	21	12	26	24	17	50	31	34	30	41	0	0
	3.75	0	0	0	0	0	0	0	46	29	12	18	24	19	20	0	32	20	18	0	0
	4.25	0	0	0	0	0	0	0	0	23	13	13	21	14	39	0	0	0	0	0	0
	4.75	0	0	0	0	0	0	0	0	39	13	21	23	22	21	0	0	0	0	0	0
	5.25	0	0	0	0	0	0	0	0	24	13	13	30	32	22	23	0	0	0	0	0
	5.75	0	0	0	0	0	0	0	0	0	43	39	0	31	0	36	0	0	0	0	0
	6.25	0	0	0	0	0	0	0	0	0	40	24	0	49	0	18	0	0	0	0	0
	6.75	0	0	0	0	0	0	0	0	28	0	0	0	0	0	0	0	0	0	0	0

Table 15: ER between the aggregate spectrum and the representative spectrum (Campbell Buoy)

		Wave Energy Period (Te)																
		0.5	1.5	2.5	3.5	4.5	5.5	6.5	7.5	8.5	9.5	10.5	11.5	12.5	13.5	14.5	15.5	16.5
Wave Height (Hmo)	0.25	4.6	0	0	0	4.6	1.4	2.7	1.1	4	1.1	1.1	1.3	1.4	0	0	0	0
	0.75	0	0	0	1.1	1.5	1	1	1	1	1.5	1.7	1	1	1	1	1	0
	1.25	0	0	0	0	1.6	1.5	1	1	1	1.2	1.3	1.5	1	1.5	0	0	0
	1.75	0	0	0	0	0	1	1	1	1	1	1.1	1	1.1	1.8	2.7	0	0
	2.25	0	0	0	0	0	0	1	1	1	1	1.1	1.4	1.2	1.5	1.6	0	0
	2.75	0	0	0	0	0	0	1	1	1	1	1	1.2	1.7	1.3	1.6	0	2.7
	3.25	0	0	0	0	0	0	0	1	1	1	1.2	1.6	1.9	1.6	1.8	0	0
	3.75	0	0	0	0	0	0	0	0	0	0	0	0	0	0	1.6	0	0

Table 16: Gamma values for representative spectrum (Renfrew Buoy)

		Wave Energy Period (Te)																
		0.5	1.5	2.5	3.5	4.5	5.5	6.5	7.5	8.5	9.5	10.5	11.5	12.5	13.5	14.5	15.5	16.5
Wave Height (Hmo)	0.25	100	0	0	0	73	61	61	60	67	63	62	67	79	0	0	0	0
	0.75	0	0	0	46	22	44	142	46	25	16	22	60	185	138	135	139	0
	1.25	0	0	0	0	29	33	141	42	16	18	17	23	23	16	0	0	0
	1.75	0	0	0	0	0	86	50	36	24	16	12	12	20	13	31	0	0
	2.25	0	0	0	0	0	0	39	49	53	28	19	14	14	13	17	0	0
	2.75	0	0	0	0	0	0	55	34	53	32	40	27	23	16	17	0	49
	3.25	0	0	0	0	0	0	0	63	40	47	44	29	15	20	19	0	0
	3.75	0	0	0	0	0	0	0	0	0	0	0	0	0	0	37	0	0

Table 17: ER between the aggregate spectrum and the representative spectrum (Renfrew Buoy)

West Coast Wave Initiative

University of Victoria
Institute for Integrated Energy Systems

Wave Energy Period (Te)

Hmo \ Te	0.5	1.5	2.5	3.5	4.5	5.5	6.5	7.5	8.5	9.5	10.5	11.5	12.5	13.5	14.5	15.5	16.5	17.5	18.5	19.5
0.25	0	0	0	0	0	0	0	0	6.5	4.6	1.1	0	0	0	0	0	0	0	0	0
0.75	0	0	0	0	1.2	1	1	1	1	1	1	1	1.6	1	1	5.1	3.3	0	0	0
1.25	0	0	0	0	1.3	1	1	1	1	1	1	1.2	1	1	1.3	1	2.6	1	0	0
1.75	0	0	0	0	0	1	1	1	1	1	1	1	1.5	1.3	1.7	2.7	0	2.7	0	0
2.25	0	0	0	0	0	3	1	1	1	1	1	1.2	1.4	1	1	2.8	4.7	0	1	0
2.75	0	0	0	0	0	2.4	1.3	1	1	1.1	1	1.3	1.7	1	1.4	1.8	1.3	2.1	0	0
3.25	0	0	0	0	0	0	3.8	1	1	1	1	1.4	1.6	1.3	2.1	2.4	2.7	0	0	0
3.75	0	0	0	0	0	0	0	2.6	1	1.2	1	1.4	1.6	1.8	1.4	2.4	3.2	6.4	4.9	0
4.25	0	0	0	0	0	0	0	0	1	1.4	1	1.5	1.6	2.2	2.5	2.4	0	5.3	0	0
4.75	0	0	0	0	0	0	0	0	1.8	1.3	1	1.4	1.7	2.2	2	4.5	7	4.1	0	0
5.25	0	0	0	0	0	0	0	0	3.1	1.4	1.3	1.4	1.9	2	1.3	1	7	0	0	0
5.75	0	0	0	0	0	0	0	0	0	2	1.6	1.3	1.9	2.1	2.3	0	5.4	0	0	0
6.25	0	0	0	0	0	0	0	0	0	0	1	1	1.5	1.5	2.8	0	0	0	0	0
6.75	0	0	0	0	0	0	0	0	0	0	1	0	3.1	2.5	1.9	2.9	0	0	0	0
7.25	0	0	0	0	0	0	0	0	0	0	1.2	1	4.4	1.4	3.1	0	0	0	0	0
7.75	0	0	0	0	0	0	0	0	0	0	0	2.6	0	2.7	0	0	0	0	0	0
8.25	0	0	0	0	0	0	0	0	0	0	0	0	0	1.8	1.6	0	0	0	0	0
8.75	0	0	0	0	0	0	0	0	0	0	0	0	0	0	0	0	0	0	0	0

Table 18: Gamma values for representative spectrum (Beverly Buoy)

Wave Energy Period (Te)

Hmo \ Te	0.5	1.5	2.5	3.5	4.5	5.5	6.5	7.5	8.5	9.5	10.5	11.5	12.5	13.5	14.5	15.5	16.5	17.5	18.5	19.5
0.25	0	0	0	0	0	0	0	0	65	62	64	0	0	0	0	0	0	0	0	0
0.75	0	0	0	0	44	78	39	41	80	49	27	65	35	47	61	33	60	0	0	0
1.25	0	0	0	0	45	44	37	36	39	47	48	15	84	49	29	56	45	72	0	0
1.75	0	0	0	0	0	36	28	27	18	16	35	24	13	45	24	73	0	49	0	0
2.25	0	0	0	0	0	52	29	20	20	19	14	17	16	35	61	25	20	0	63	0
2.75	0	0	0	0	0	50	23	19	18	11	22	17	15	31	37	41	59	39	0	0
3.25	0	0	0	0	0	0	40	41	11	10	13	19	19	21	24	14	32	0	0	0
3.75	0	0	0	0	0	0	0	29	22	10	23	20	17	12	35	20	31	15	52	0
4.25	0	0	0	0	0	0	0	0	17	8	26	22	24	11	16	30	0	39	0	0
4.75	0	0	0	0	0	0	0	0	15	25	11	18	23	12	22	25	19	42	0	0
5.25	0	0	0	0	0	0	0	0	46	17	28	22	27	12	40	114	37	0	0	0
5.75	0	0	0	0	0	0	0	0	0	10	27	20	19	18	17	0	20	0	0	0
6.25	0	0	0	0	0	0	0	0	0	0	69	19	16	19	20	0	0	0	0	0
6.75	0	0	0	0	0	0	0	0	0	0	23	0	14	26	21	29	0	0	0	0
7.25	0	0	0	0	0	0	0	0	0	0	23	42	21	21	20	0	0	0	0	0
7.75	0	0	0	0	0	0	0	0	0	0	0	48	0	31	0	0	0	0	0	0
8.25	0	0	0	0	0	0	0	0	0	0	0	0	0	13	15	0	0	0	0	0
8.75	0	0	0	0	0	0	0	0	0	0	0	0	0	0	0	0	0	0	0	0

Table 19: ER between the aggregate spectrum and the representative spectrum (Beverly Buoy)

Wave Energy Period (Te)

Hmo \ Te	0.5	1.5	2.5	3.5	4.5	5.5	6.5	7.5	8.5	9.5	10.5	11.5	12.5	13.5	14.5	15.5	16.5	17.5
0.25	0	0	0	0	0	0	0	1.7	1.1	4.2	1.1	4.6	4.6	0	0	0	0	0
0.75	0	0	0	0	0	1	1	1	1	1	1	1.8	2.5	0	0	0	0	0
1.25	0	0	0	0	1	1	1	1	1	1	1	1.1	1	1.2	2.1	0	0	1.2
1.75	0	0	0	0	0	1.1	1	1	1	1.1	1	1.4	1.2	1	1	0	0	0
2.25	0	0	0	0	0	1.9	1.1	1	1	1.1	1.1	1.3	1.3	1	1	0	0	0
2.75	0	0	0	0	0	0	1.3	1	1	1.1	1.2	1.2	1.5	1	1	2.6	2.5	0
3.25	0	0	0	0	0	0	1.4	1	1	1.2	1.3	1.5	1.3	1.6	1.9	2.6	4	0
3.75	0	0	0	0	0	0	0	1	1.1	1.3	1.4	1.5	2	0	2.4	4	3	0
4.25	0	0	0	0	0	0	0	0	1.4	1.4	1.6	1.3	0	0	0	0	0	0
4.75	0	0	0	0	0	0	0	0	2.1	1.5	1.5	1.5	2.9	0	0	0	0	0
5.25	0	0	0	0	0	0	0	0	0	2	1.7	2.3	1.6	1	0	0	0	0
5.75	0	0	0	0	0	0	0	0	0	0	5.5	1.7	1.5	1.6	0	0	0	0
6.25	0	0	0	0	0	0	0	0	0	0	0	2.9	1	1.7	2	0	0	0
6.75	0	0	0	0	0	0	0	0	0	0	0	1.3	1.2	0	0	0	0	0

Table 20: Gamma values for representative spectrum (Tarbotton Buoy)

University of Victoria
Institute for Integrated Energy Systems

		0.5	1.5	2.5	3.5	4.5	5.5	6.5	7.5	8.5	9.5	10.5	11.5	12.5	13.5	14.5	15.5	16.5	17.5
	0.25	0	0	0	0	0	0	0	79	62	72	68	59	66	0	0	0	0	0
	0.75	0	0	0	0	0	46	34	44	98	72	44	32	43	0	0	0	0	0
	1.25	0	0	0	0	67	28	41	37	31	30	28	12	71	71	55	0	0	53
	1.75	0	0	0	0	0	26	32	27	18	14	17	10	13	59	64	0	0	0
	2.25	0	0	0	0	0	23	20	35	20	12	12	13	20	44	56	0	0	0
Wave Height (Hmo)	2.75	0	0	0	0	0	0	20	17	21	13	11	12	13	25	21	47	32	0
	3.25	0	0	0	0	0	0	63	25	13	11	10	9	17	18	10	17	37	0
	3.75	0	0	0	0	0	0	0	26	30	11	16	8	12	0	26	27	27	0
	4.25	0	0	0	0	0	0	0	0	19	7	13	9	25	0	0	0	0	0
	4.75	0	0	0	0	0	0	0	0	24	26	10	14	10	0	0	0	0	0
	5.25	0	0	0	0	0	0	0	0	0	18	15	12	12	68	0	0	0	0
	5.75	0	0	0	0	0	0	0	0	0	0	13	9	13	19	0	0	0	0
	6.25	0	0	0	0	0	0	0	0	0	0	0	17	40	18	42	0	0	0
	6.75	0	0	0	0	0	0	0	0	0	0	0	0	18	18	0	0	0	0

Table 21: ER between the aggregate spectrum and the representative spectrum (Tarbotton Buoy)

2.4 Bivariate Histogram Uncertainty Analysis Conclusions and Recommendations

Through a systematic analysis of the wave spectrums measured by the four WCWI wave measurement buoys, it was shown that, on aggregate, a PM spectrum best represents the incident wave spectrum off the British Columbia coast. However, as the wave energy period increases, the spectral shapes become increasingly peaked and closer to a JONSWAP spectrum.

With regards to the RMS relative error, or uncertainty, associated with the "best-fit" single peaked wave spectrums for each wave height/energy period bin, it was noted that lower wave heights generally featured higher ER values. These increased ER values may be attributed to multi-peaked wave spectrums, as illustrated in Figure 23, and it is recommended that further research is conducted into partitioning of the incoming wave spectrums into discrete single peaks. This work is beyond the scope of this report yet is important to reduce the uncertainties associated with both gross resource and WEC power production estimates.

3 Wave/WEC Interactions and WEC Array Modeling Methodologies

For the Wave/WEC Interaction and Array Methodology research, the objective was to develop an initial methodology to account for WEC interactions, available wave resources within WEC farms and the transformation changes to the wave climate. This effort was conducted in collaboration with Sandia National Labs and utilized their SNL-SWAN code.

Sandia National Laboratories (SNL) SWAN is a modified version of the baseline SWAN model. WCWI gained access to this model through a collaboration with SNL of Albuquerque, USA. SNL-SWAN is designed to help quantify the effects of wave energy converter farms on the near and far field wave conditions. To date, most wave energy conversion farms have been simply modelled as obstacles similar to breakwaters within SWAN. As part of this method, the transmission of wave energy through an obstacle is been constant and independent the incident frequency of the waves. This approach is limited, given that wave power absorption is correlated to both with the incident power and the device's performance in particular sea states. SNL-SWAN provides a number of options to implement frequency dependent power absorption.

In order to implement the SNL-SWAN code, a high resolution SWAN model of the Ucluelet area was produced to allow for the inclusion of WEC's within the SWAN environment. Next, a frequency domain response curve for the UVic two-body point absorber was developed to characterize WEC performance. Finally, the WEC response curve was utilized within the Scandia National Labs SNL-SWAN model to determine influence on WEC farms on annual wave climate.

3.1 Development of High Resolution SWAN Model of Possible WEC Deployment Sites

In order to account for the integration of numerous WEC's within the SWAN wave model, increased spatial resolution of the computational grid was required. Two grids with different resolution were developed, shown below, in an effort to characterize the coastline from Tofino to Ucluelet, including regions of Clayoquot Sound and Barkley Sound. The area covers 2,343.4 km^2 and extends 38 km offshore. This location was chosen due to continued interest from WEC developers in the sites of Florencia Bay and Amphitrite Bank.

The first grid (Figure 24) has a minimum resolution of 2500 m/element along the offshore boundary and a maximum resolution of 5 m/element in areas close proposed WEC farm locations. The grid contains 67,084 nodes and 133,313 elements. This grid is capable of capturing the effects of WEC's as small as 10 m in diameter.

The second grid (Figure 25) has a minimum resolution of 1000 m/element along the offshore boundary and a maximum resolution of 5 m/element in the vicinity of the proposed WEC farm location. The grid has 97,107 nodes and 193,263 elements. The fine grid resolution also captures the effects of a wave energy converter 10 m wide but will provide additional resolution on wave spreading.

To capture the effect of single WEC's, the grid should at least 2 node crossings per WEC width. In Figure 24, the significant resolution difference between the coarsest and finest mesh areas was found to produce numerical errors in the SWAN model. The model is discussed later in this report and indicates this effect. Figure 25 was generated with a finer resolution at its coarsest element edge to in order to decrease the resolution differences in the grid; however, this resolution is significantly more computationally expensive than the coarser resolution grid.
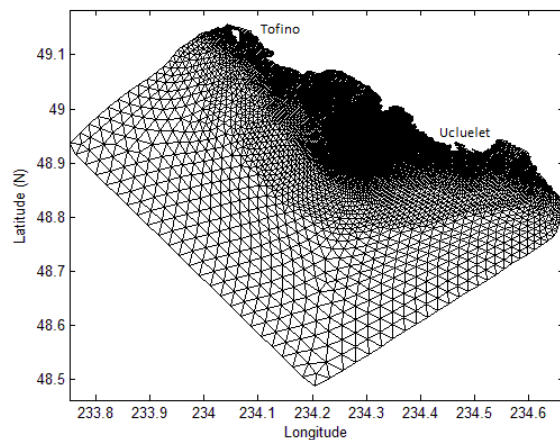
Figure 24: Coarse unstructured grid containing 67,084 computational nodes. Maximum element length of 2500 m with a maximum resolution of 5 m
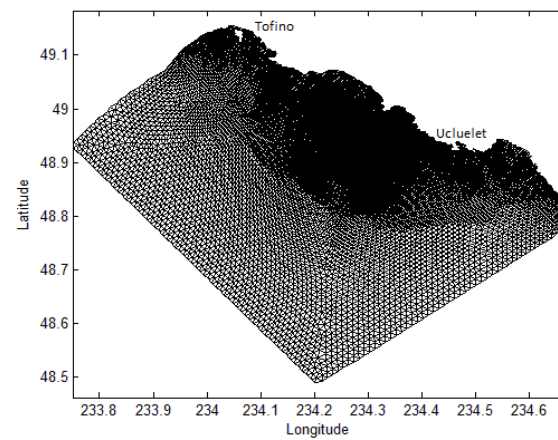
Figure 25: Fine unstructured grid containing 97,107 computational nodes. Maximum element length of 1000 m with a maximum resolution of 5 m

3.2 Normalized Frequency Domain Response Curve from WCWI WEC's Device Simulations

The WCWI WEC consists of two self-contained concentric bodies: a torus and a spar. Utilizing the time varying sea surface elevation, the two bodies move relative to each other along their combined axisymmetric axis. The WCWI WEC is based on Wavebob, a previous pre-commercial WEC concept, and is the full-scale version of the WEC used by previous research [9] [10]. Operating between the torus and spar is a power take off (PTO) device that produces a force opposing, and in proportion, to the relative velocity. The system is deployed in 50 m of sea water and is moored with a three mooring line configuration that is evenly spaced and attached to the spar at its centre of gravity. The mooring lines are composed of 81 m of chain anchored to the sea floor at a distance of 73 m from the centre of the WEC.
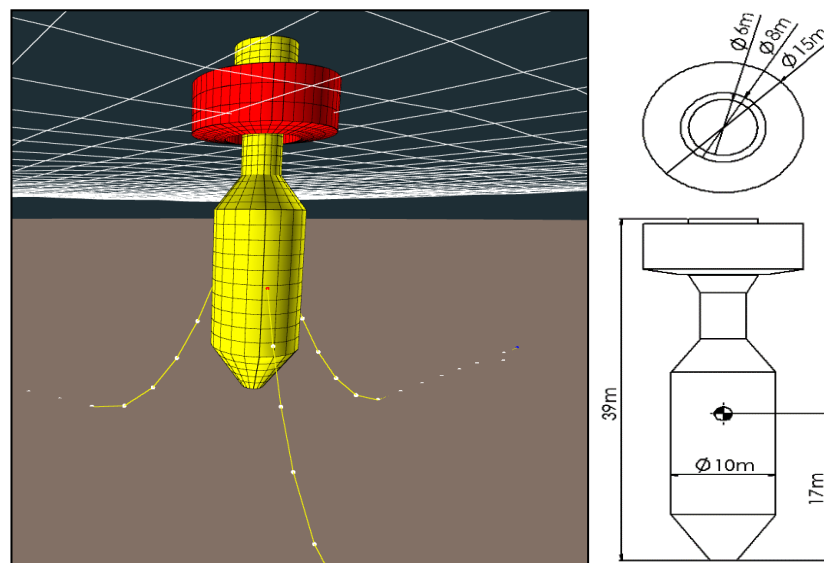

Figure 26: A visual result of the WEC simulation model in ProteusDS and the dimensioned schematics

The WEC was simulated using the commercial software package, ProteusDS [11]. ProteusDS is a non-linear, time domain, finite element, solver that operates in 6 degrees of freedom. The software's physics model has been extensively validated and includes non-linear mooring cable dynamics, inter-connections of articulate hulls and mooring lines, power take-off (PTO) dynamics, and viscous drag forces. Wave hydrodynamic information, diffraction loading and the frequency dependent add mass and added damping values have been calculated in the boundary element method code, WAMIT, and used within the ProteusDS environment [11] [12]. The parameters used in the model are presented in Table 22.

Parameters	Unit	Value
Spar Mass	Kg	1646875
Spar Moments of Inertia: Ixx, Iyy, Izz	Kgm^2	5656250, 5656250, 648437.5
Float Mass	Kg	201406.25
Float Moments of Inertia: Ixx, Iyy, Izz	Kgm^2	5785156.25, 5785156.25, 1445312.5
Chain Density	Kg/m^3	7700
Chain effective diameter	m	0.03655
Chain Axial rigidity	N	4.2x10^8
PTO damping coefficient	Ns/m	1625 000

Table 22: WEC numerical model parameters

The WEC power matrix shown in Figure 27 presents the power production (W) for the individual sea state measured by the Beverly buoy.

Sig. Wave Height	4-4.9	5-5.9	6-6.9	7-7.9	8-8.9	9-9.9	10-10.9	11-11.9	12-12.9	13-13.9	14-14.9	15-15.9	16-16.9	17-17.9	18-18.9
7-7.4							382273	316690	315451		182624				
6.5-6.9							307455			196419	196427	171433			
6-6.4							335479	243487	233754	190112	155998				
5.5-5.9						350509	281937	245508	181892	181085	117726		96551		
5-5.4						251154	202664	215636	171320	106898	109648		81939		
4.5-4.9					216348	286642	249968	169236	144903	129329				55973	
4-4.4				199997	252618	223552	188520	162766	120977	90174	89048	64442			43151
3.5-3.9				205640	205259	190768	151211	120438	139172	70271	69299	60085	47136	34246	36314
3-3.4			165575	171086	169001	181686	131727	76295	75572	82253	49809	37663	34474		
2.5-2.9			139140	116106	102995	92764	69306	75712	51381	53840	39425	30785	25044	19907	
2-2.4			96337	81287	76425	72518	65939	51369	34558	33246	19127	22967		13696	
1.5-1.9		41874	49763	62589	55531	47239	31388	33595	26451	23563	13695	10473	10503		7177
1-1.4	17296	16172	30548	24410	24258	18210	22051	15466	14474	14474	14474	14474	14474	14474	14474
0.5-0.9	6720	7053	9134	10781	8337	7480	8738	5281	10695	8866	7567				
0-0.4				1155	1092	874	556	561	477	357					

Energy Period (s)

Figure 27: Power matrix for WCWI concept WEC given in watts

In Figure 28, a frequency domain response curve, normalized by the wave power present in the appropriate frequency bin, is presented based on the ProteusDS simulations of the device in different irregular sea states. The standard deviation (STD) lines represent the variation in the ratio of absorbed power to incident wave power, over the full range of wave heights for each frequency. This curve is utilized by SNL-SWAN to account for the amount of power "absorbed" by individual WEC's.
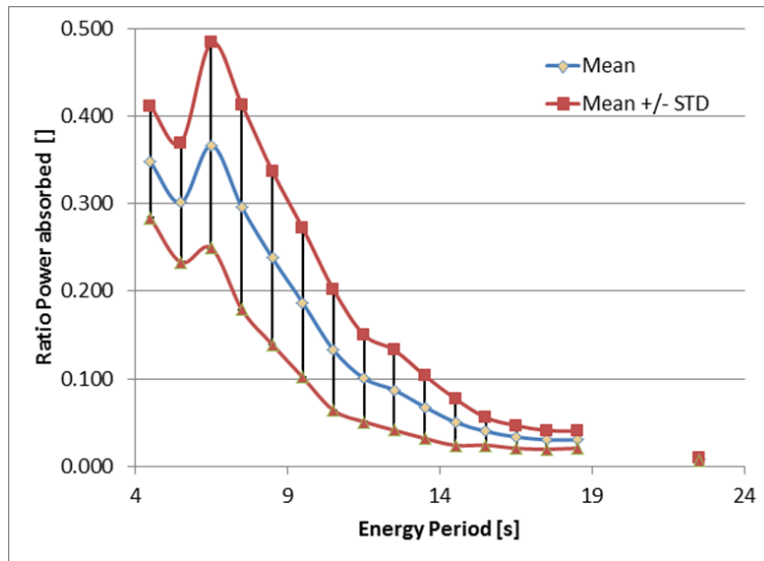
Figure 28: Normalized frequency domain response curve

3.3 Demonstration Wave Array within SWAN Model and Influence on Annual Wave Climate

Transmission coefficients for use within SNL-SWAN can be determined by taking the ratio between the power absorbed and the incident power at that particular sea state, where K_t represents the transmission coefficient, P_{inc} represents the incident wave power and P_{lee} is the wave power in the lee of the WEC farm:

$$\frac{P_{inc} - P_{lee}}{P_{inc}} = \frac{P_{abs}}{P_{inc}} = K_t^2 \tag{8}$$

SNL-SWAN currently has five different obstacle cases available to determine the effects of WEC farms of the wave climate. Within these five obstacle cases, SNL-SWAN uses three different methods to determine power absorption of an obstacle. The different obstacle cases and how they are used by the software are outlined in the table below:

Obstacle Case Number	Description
0	Constant transmission coefficient (entered directly in the input file)
1	Finds the power absorption value for the peak period within a sea state. A single transmission coefficient is calculated for this period and corresponding significant wave height. Applies uniformly across the wave spectrum
2	A relative capture width curve calculates a single transmission coefficient that is applied uniformly across the wave spectrum
3	Finds the row in a power matrix associated with the significant wave height of a sea state. A transmission coefficient is calculated for each period within a sea state, at the known significant wave height, and applied to each frequency bin within the wave spectrum. Results in variations in power absorption across the wave spectrum.
4	Calculates a transmission coefficient for every frequency bin within a wave spectrum, creating frequency dependent power absorption.

Table 23: Description for each obstacle case

At present, obstacle cases 0,1 and 3 have been investigated in order to determine SNL SWAN's performance with respect to a power matrix. The plot below demonstrates how the spectrum in the lee of a wave energy converter (50 m behind WEC) is affected by using different obstacle cases. The original spectrum unaffected by the obstacle is presented in black. All three obstacle cases extract power from the spectrum, however the range of power absorption varies with each case. Using a transmission coefficient that removes the same amount of energy regardless of the sea state overpredicts the amount of energy extracted from higher sea states and underpredicts the energy extracted in less energetic sea states. Constant transmission does not accurately convey device performance in specific sea states.
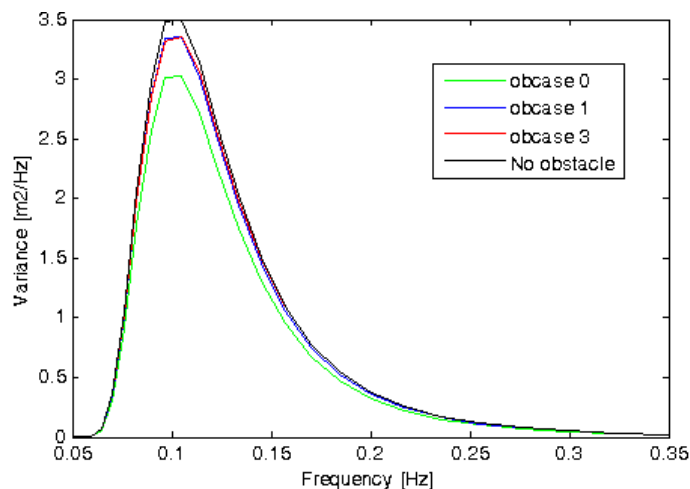

Figure 29: Wave spectrum in the lee of a WEC

The effect of using frequency dependent absorption can be demonstrated further by looking at the change in significant wave height induced in the lee of a wave energy converter using obstacle cases 0 and 1. For the purposes of these scenarios, a single transmission coefficient was generated for input in obstacle case 0 by determining the incident power at an obstacle for every sea state modelled using a Pierson-Moskowitz spectrum. The power absorbed at the corresponding sea state was extracted from a power matrix. A transmission coefficient was calculated for each sea state and a weighted average of the transmission coefficients was taken based on how often that particular sea state occurred.

The mean transmission coefficient was compared to the implementation of a frequency dependent transmission coefficient in the most energetic sea state recorded at Amphitrite Bank in 2008. The results below indicate that using a single transmission coefficient over predicts the reduction in wave height associated with a wave energy converter. The difference in wave height in the lee of the wave energy converters is 1.5 m. Obstacle cases 1 and 3 are more accurate representations of the device's performance in that particular sea state. Results are shown on the figures below. Note the colour scale is modified in Figure 31 and Figure 32 to obtain a better visualization for case 1 and case 3. For obstacle case 1, the relative change is only 0.06 m and only 0.03 m for obstacle case 3.

The changes in power absorption between the three cases have a cumulative effect over time. The power absorbed by an obstacle with a constant transmission coefficient will be much larger over time. The table below presents the energy absorbed over the course of a year by an obstacle. These values have been generated by multiplying the power absorbed in each sea state by the number of hours they occur in a year. The energy absorbed by obstacle 0 is an order of magnitude larger than the other two cases.

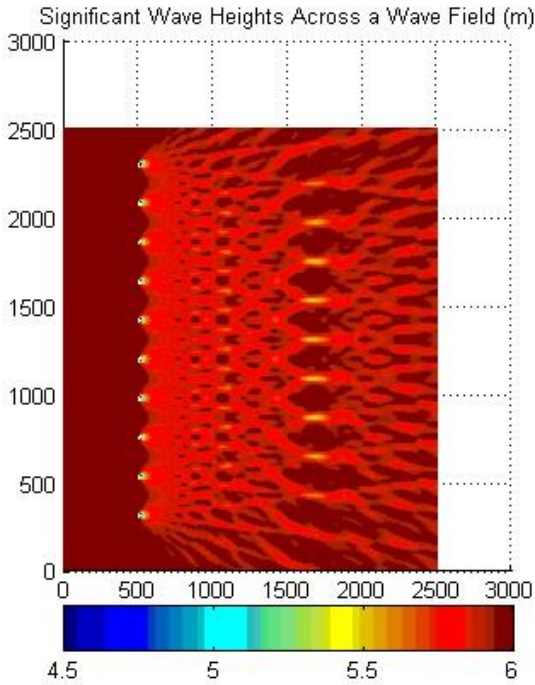|	Obstacle Case 0	Obstacle Case 1	Obstacle Case 3
Energy Absorbed	3.11 MWhr	0.58 MWhr	0.40 MWhr

Table 24: Power absorbed per year

Figure 30: Significant wave height across a wave field for obstacle case 0
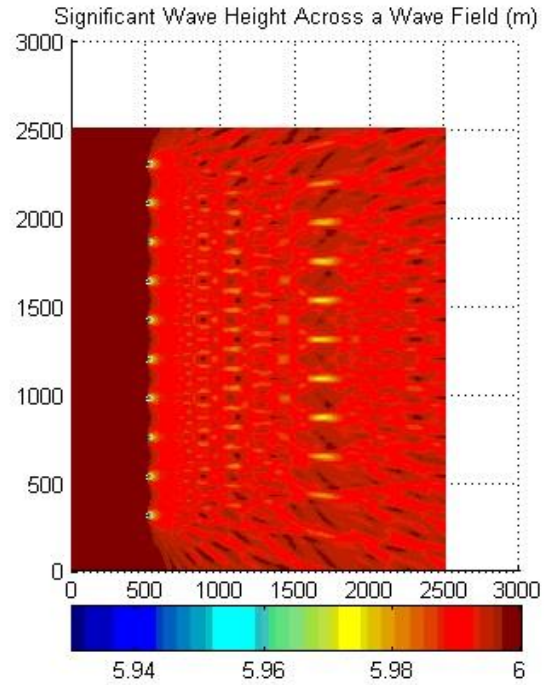

Figure 31: Significant wave height across a wave field for obstacle case 1 with modified color scale
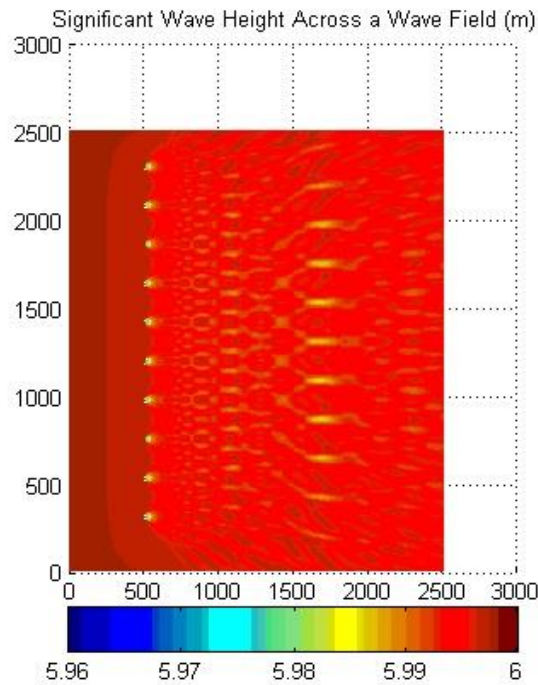

Figure 32: Significant wave height across a wave field for obstacle case 3 with modified color scale

3.4   Wave/WEC Array Analysis Conclusions and Recommendations

Initial investigations into the implementation of WEC arrays within the SWAN model highlighted the necessity for highly resolved computational grids in the vicinity of the WEC array. These are necessary to resolve the WEC array interactions and the effect of the local wave climate. It is suggested that a minimum of two (2) numerical grid crossings per WEC diameter are required to capture the effect of the WEC on the wave climate. Four (4) to five (5) grid crossing are recommended.

Frequency domain WEC response curve (shown in Figure 29) presents an additional representation of WEC performance and allow for implementation within the Scandia National Labs SNL-SWAN code. Five obstacle cases are allowable in SNL-SWAN, with each subsequent obstacle case allowing for improvements in the precision of the WEC representation. As shown in Figure 30, Figure 31 and Figure 32, the initial model results appear favourable and illustrate the differences between each obstacle case.

Further development and refinement of WEC arrays within numerical wave models is vital to the quantifying the effects of WEC arrays on the local wave climate. These models provide the baseline tool and knowledge to start understanding the ecological ramifications of large scale WEC deployment. This work needs to continue within the Canada in order to reduce the perceived risks to WEC deployments and identify the real risks. With these goals in mind, WCWI is currently working with SNL to include all non-power generation losses in the assessment of power removed from the wave field, and including WEC-induced waves into SNL-SWAN environment.

4   Mooring Design and Load Data Collection

For Mooring Design and Load Data Collection research, the objective was to acquire mooring line load data and TRIAXYS buoy motions for future analysis by TC-114 terms. The combination of high resolution characterizations of wave condition data at the collocated TRIAXYS/AWAC location provides the perfect test site for the collection of full-scale real world mooring line load data.

Working in partnership with AXYS Technologies, WCWI personnel specified and installed a load cell in line with a traditional AXYS Technologies buoy mooring system and an extensive dataset of mooring loads under regular operation was collected. The novel integration of the mooring load data into the WatchMate 500 module, allowing for real-time mooring load data access, will prove to be invaluable when full scale WEC deployments occur.

4.1   Design and install Load Cell and Data Acquisition System for TRIAXYS Mooring Line

A custom load cell was developed by Sensing System Corporation (SSC) as per the design requirements from WCWI. The design requirements were determined through site studies and detailed numerical simulation of the wave loading on a TriAxys buoy using ProteusDS. SSC provided a load cell with a full scale capacity of 5000 lbs, utilizing a 0.1 to 5.1 VDC output from an integral amplifier. The specifications for the load cell and amplifier are shown in Table 25 and Table 26 below:

Model:	Custom Tension Link Load Cell
Capacity:	5,000 Lbs Full Scale (FS)
Safe Overload:	150% of FS
Load Cell Output:	1.5 m V/V nominal at FS
Amplified Output:	0.1 to 5.1 VDC with Integral Amplifier
Accuracy/Combined Errors:	0.25% of FS
Material:	17-4 PH stainless steel
Cable/Connector:	Subconn bulkhead, connector type MCBH4FSS. Mating Connector with 1 m long pigtail and flying leads.
Load Cell Size:	2.5 inch Diameter by 8.625 inch length
Attachments:	0.875 inch Through Hole on each end for shackles

Table 25 Load cell specifications

Model	SSC-ICA2H
Supply Voltage:	8.5-28 VDC
Operating Current:	23mA
Output Signal:	0.1-5.1 VDC
Linearity	0.02% of Full Scale
Bandwidth	DC to 1 ,000 Hz
Bridge Excitation	5VDC

Table 26: Integral amplifier specifications

Instead of providing a dedicated power supply and data acquisition system for the load cell, WCWI worked with AXYS Technologies to integrate the load cell data power and data into the TriAxys buoy data collection system and transmit real-time data back to shore through a satellite data transfer system. This novel mooring load and wave measurement system will be useful to future WEC developers as the need to better understand real-time mooring dynamics during full scale deployments.

A drawing for the TRIAXYS mooring and generic load cell are included below. The load cell was mounted at position (2) in Figure 33. Figure 35 and Figure 36 provide images of the actual load cell mounting.
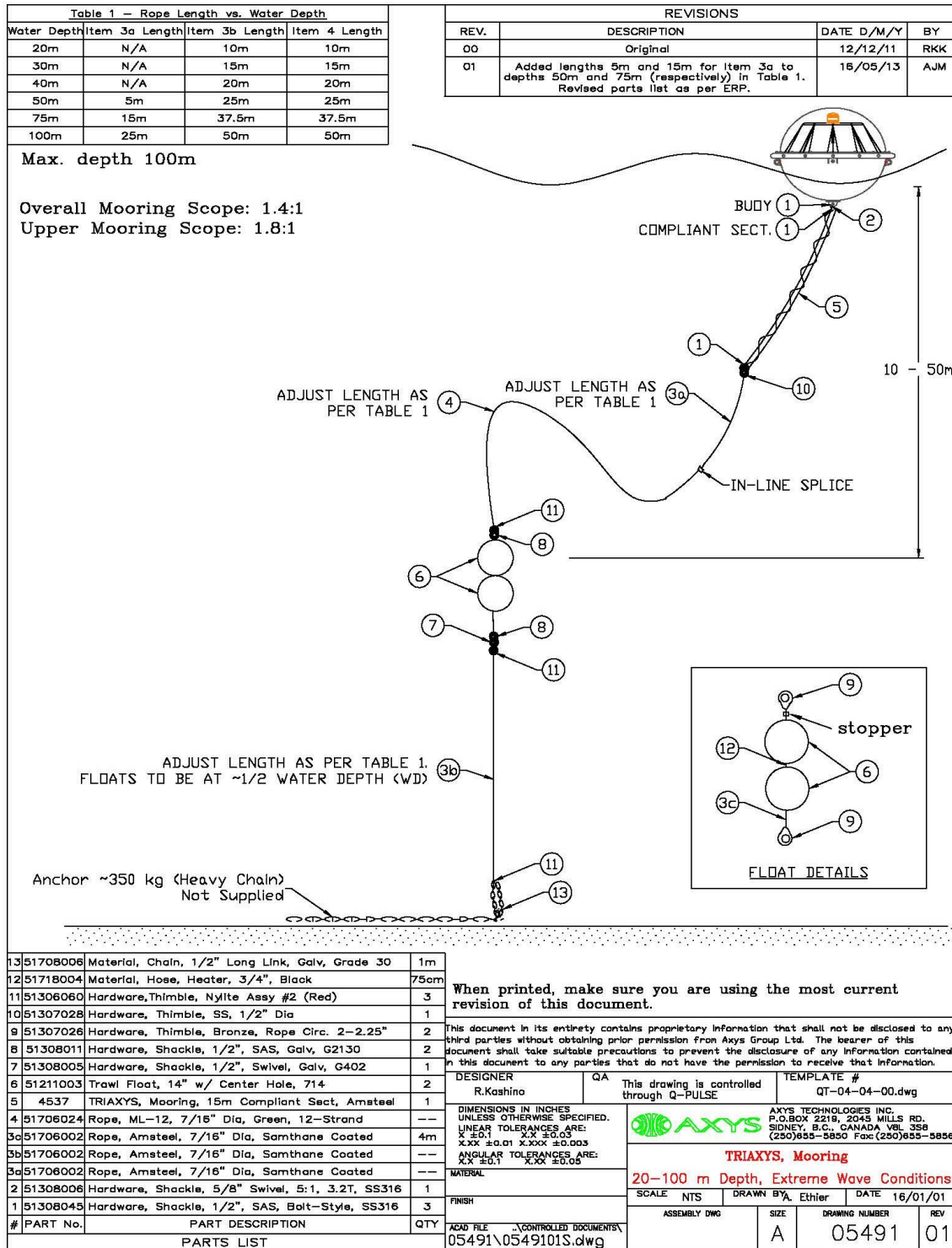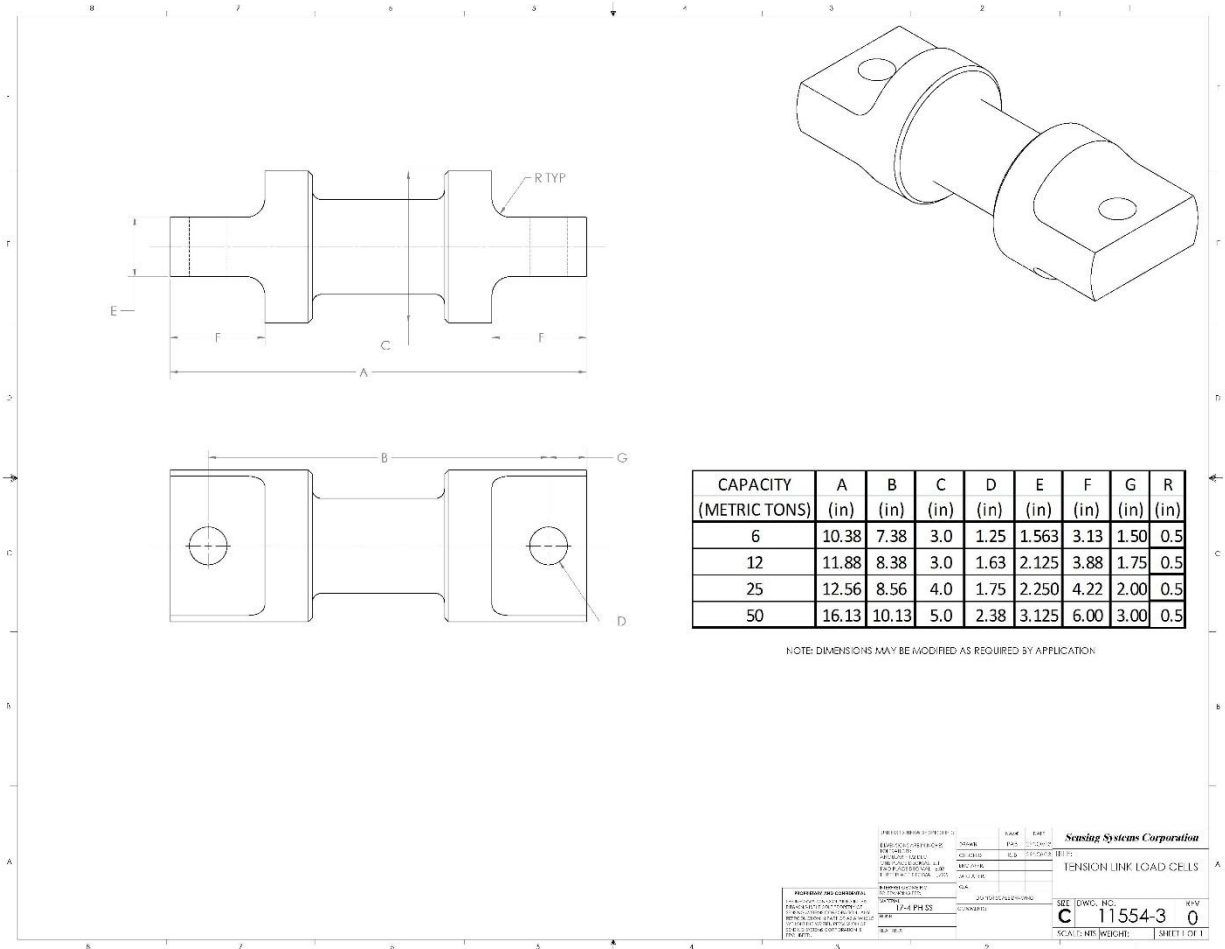

Table 1 — Rope Length vs. Water Depth

Water Depth	Item 3a Length	Item 3b Length	Item 4 Length
20m	N/A	10m	10m
30m	N/A	15m	15m
40m	N/A	20m	20m
50m	5m	25m	25m
75m	15m	37.5m	37.5m
100m	25m	50m	50m

Max. depth 100m

Overall Mooring Scope: 1.4:1
Upper Mooring Scope: 1.8:1

REVISIONS

REV.	DESCRIPTION	DATE D/M/Y	BY
00	Original	12/12/11	RKK
01	Added lengths 5m and 15m for Item 3a to depths 50m and 75m (respectively) in Table 1. Revised parts list as per ERP.	16/05/13	AJM

PARTS LIST

#	PART No.	PART DESCRIPTION	QTY
13	51706006	Material, Chain, 1/2" Long Link, Galv, Grade 30	1m
12	51718004	Material, Hose, Heater, 3/4", Black	75cm
11	51306060	Hardware, Thimble, Nylite Assy #2 (Red)	3
10	51307028	Hardware, Thimble, SS, 1/2" Dia	1
9	51307026	Hardware, Thimble, Bronze, Rope Circ. 2-2.25"	2
8	51308011	Hardware, Shackle, 1/2", SAS, Galv, G2130	2
7	51308005	Hardware, Shackle, 1/2", Swivel, Galv, G402	1
6	51211003	Trawl Float, 14" w/ Center Hole, 714	2
5	4537	TRIAXYS, Mooring, 15m Compliant Sect, Amsteel	1
4	51706024	Rope, ML-12, 7/16" Dia, Green, 12-Strand	--
3c	51706002	Rope, Amsteel, 7/16" Dia, Samthane Coated	4m
3b	51706002	Rope, Amsteel, 7/16" Dia, Samthane Coated	--
3a	51706002	Rope, Amsteel, 7/16" Dia, Samthane Coated	--
2	51308006	Hardware, Shackle, 5/8" Swivel, 5:1, 3.2T, SS316	1
1	51308045	Hardware, Shackle, 1/2", SAS, Bolt-Style, SS316	3

When printed, make sure you are using the most current revision of this document.

This document in its entirety contains proprietary information that shall not be disclosed to any third parties without obtaining prior permission from Axys Group Ltd. The bearer of this document shall take suitable precautions to prevent the disclosure of any information contained in this document to any parties that do not have the permission to receive that information.

DESIGNER: R.Kashino
This drawing is controlled through Q-PULSE
TEMPLATE #: QT-04-04-00.dwg

DIMENSIONS IN INCHES UNLESS OTHERWISE SPECIFIED.
LINEAR TOLERANCES ARE:
X ±0.1   X.X ±0.03
X.XX ±0.01 X.XXX ±0.003
ANGULAR TOLERANCES ARE:
X.X ±0.1   X.XX ±0.05

AXYS TECHNOLOGIES INC.
P.O.BOX 2219, 2045 MILLS RD.
SIDNEY, B.C., CANADA V8L 3S8
(250)655-5850 Fax (250)655-5856

TRIAXYS, Mooring
20-100 m Depth, Extreme Wave Conditions

SCALE: NTS   DRAWN BY: A. Ethier   DATE: 16/01/01
ASSEMBLY DWG   SIZE: A   DRAWING NUMBER: 05491   REV: 01
ACAD FILE: ..\CONTROLLED DOCUMENTS\05491\0549101S.dwg

Figure 33: Mooring line schematic

Figure 34: Load cell generic drawing

CAPACITY (METRIC TONS)	A (in)	B (in)	C (in)	D (in)	E (in)	F (in)	G (in)	R (in)
6	10.38	7.38	3.0	1.25	1.563	3.13	1.50	0.5
12	11.88	8.38	3.0	1.63	2.125	3.88	1.75	0.5
25	12.56	8.56	4.0	1.75	2.250	4.22	2.00	0.5
50	16.13	10.13	5.0	2.38	3.125	6.00	3.00	0.5

NOTE: DIMENSIONS MAY BE MODIFIED AS REQUIRED BY APPLICATION

Figure 35: Attaching load cell to the bottom of buoy

Figure 36: Connection between buoy and load cell

4.2   Collecting Data on Buoy Motions

Bin files for buoy motions were zipped and are attached to the report for detailed further analysis. The files contain data between September 25th, 2014 and October 28th, 2014. Unfortunately, the load cell data acquisition system failed on October 28th and no further information was collected. Each bin file details a single day of data from the load cell by using buoy accelerometers and rate gyros with 4Hz sampling rate. The header for each column in the bin files is shown below.

Column 1	Column 2	Column 3	Column 4	Column 5	Column 6	Column 7	Column 8	Column 9	Column 10
yymmdd	hhmmss.ms	Tension (lbs)	Direction (deg)	Ax (g)	Ay (g)	Az (g)	Rx (deg/s)	Ry (deg/s)	Rz (deg/s)

Table 27: Header for bin file

4.3   Collecting Load Data during Regular Buoy Maintenance

The load cell data contained in bin file #37 and #38 was collected between September 25th, 2014, 2035 hours and September 26th, 2014, 1000 hours. On these days, buoy transportation and deployment occurred. As noted above, the load cell data acquisition system failed on October 28th, 2014. Therefore, load data during buoy retrieval was not collected. However, data is predicted to become available after the next buoy maintenance cycle, scheduled for August, 2015.

4.4   Loads Comparison among TRIAXYS, AWAC, and SWAN Model.

The average mooring line tension, corresponding peak wave period and significant wave height from the TRIAXYS buoy, AWAC, and SWAN model are shown below. Peak wave period and significant wave height, as measured by buoy and AWAC, are shown in Figure 38 and Figure 39 respectively. In Figure 40 and Figure 41, a three hour moving average curve is presented for the AWAC and buoy data. This allows comparison against the SWAN model data, which is computed at 3 hour resolution, as per Section 2.
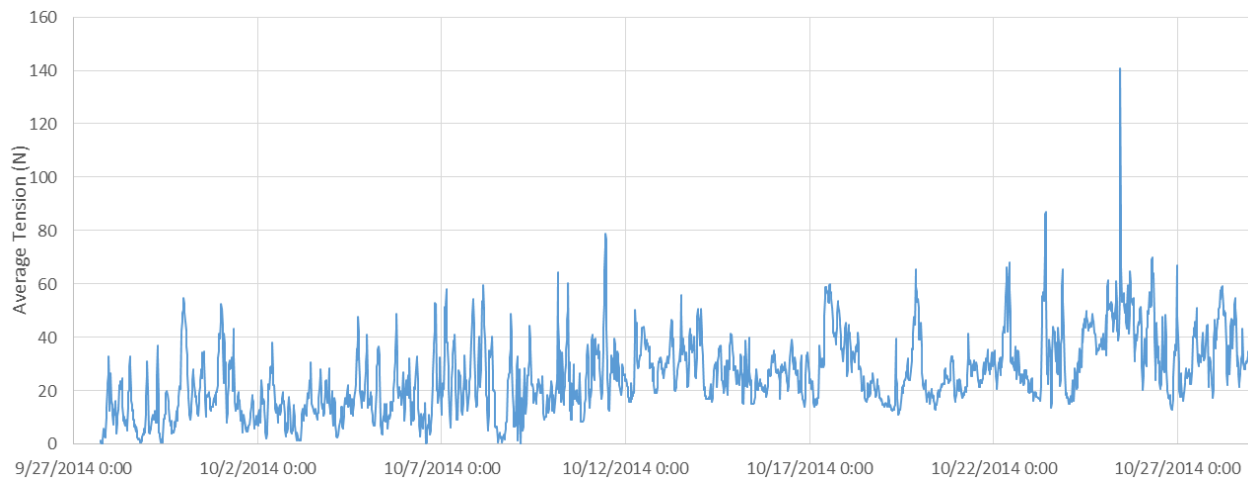

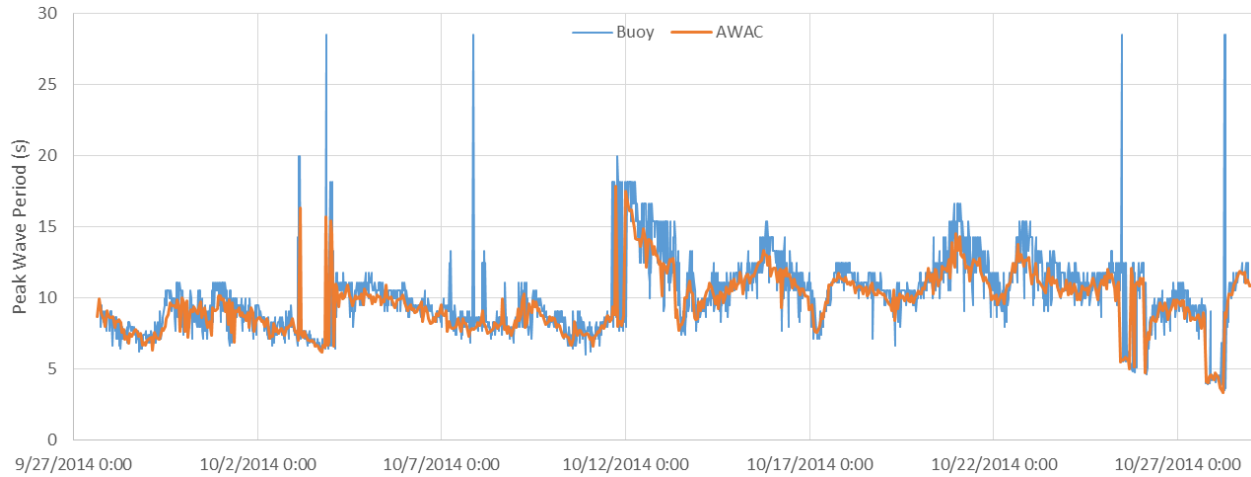**Figure 37: Average mooring line tension**

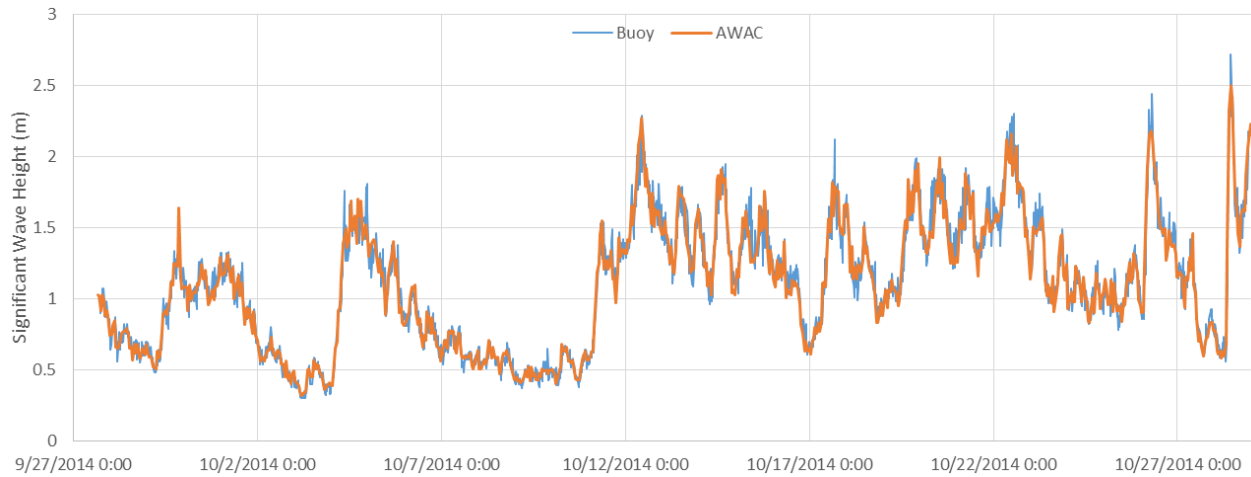**Figure 38: Peak wave period for the Renfrew buoy and AWAC**

Figure 39: Significant wave height for the Renfrew buoy and AWAC
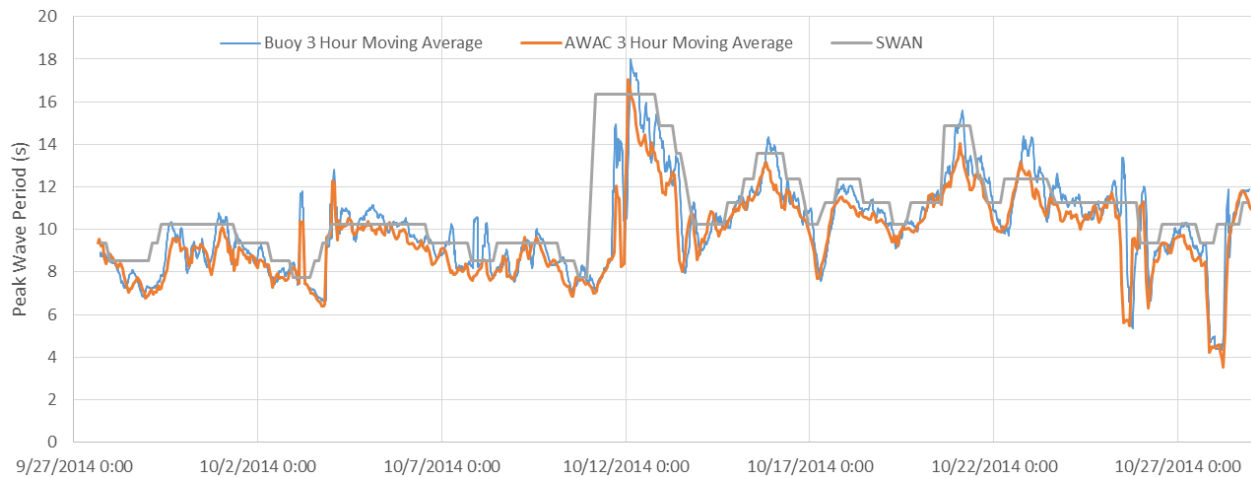

Figure 40: Peak wave period with three hour time step for the Renfrew buoy, AWAC, and SWAN model
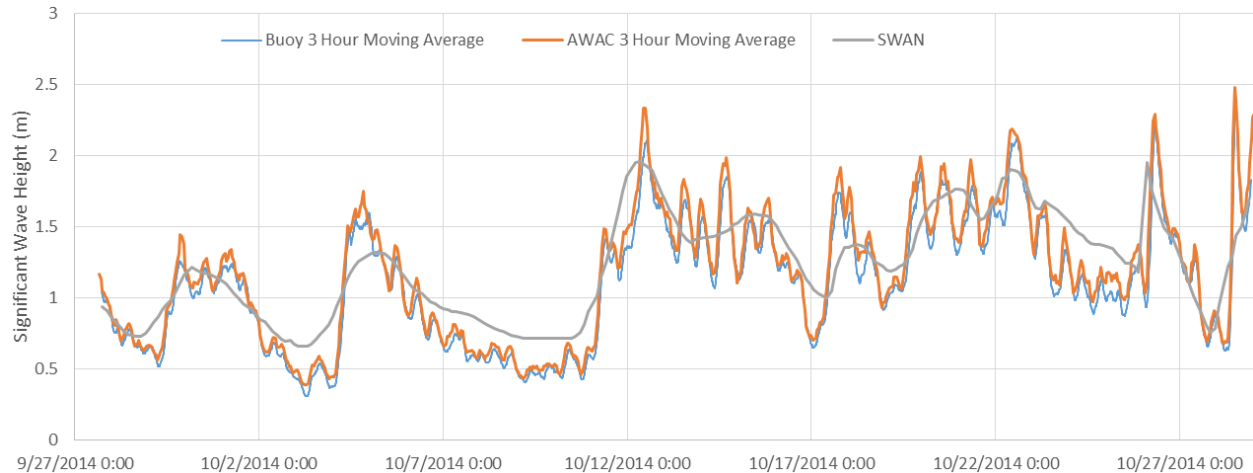
Figure 41: Significant wave height with three hour time step for the Renfrew buoy, AWAC, and SWAN model

4.5   Mooring Design and Load Data Collection Conclusions

Utilizing ProteusDS simulations of extreme mooring loads on a TriAxys wave measurement buoy, WCWI working in collaboration with Axys Technologies and Sensing Systems Inc to design and install a load cell into their standard marine mooring. The novel integration of a load cell within the data acquisition and data transmission system of the TriAxys buoy allowed WCWI researchers to access real-time wave and load measurements. As the WEC industry matures, the ability to monitor device loads and access maintenance requirements will provide invaluable.

Detailed analysis of the mooring load data, in concert with the SWAN, AWAC and buoy wave data, was beyond the scope of the WCWI-ERP. In the future, WCWI would welcome and opportunity to further investigate these datasets and provide detailed recommendations for standards development.

5   WCWI Extended Research Program Conclusions

The West Coast Wave Initiative (WCWI) Extended Research Program (ERP) was completed by the WCWI, a research group within the Institute for Integrated Energy Systems at the University of Victoria. The WCWI is a collaboration of university researchers, international Wave Energy Converter (WEC) developers, and Canadian service providers. The WCWI-ERP program benefitted by collaborating with AXYS Technologies, Cascadia Coastal Research Ltd, Nortek USA, Golder Associates, and Sandia National Labs.

This report details the results and findings of the WCWI-ERP in three major sections: Resource Modelling and Uncertainty Analysis, Wave/WEC interactions and Wave Farm Array Methodologies, and Mooring Design and Stress Load Data Collection. Given the breath of topics researched as part of the WCWI-ERP, the findings and basic conclusions for each section are included within the bulk of the report. Readers interested in specific findings are directed towards Table 1 and the appropriate report portion.

6 References

[1] International Electrotechnical Commission, *IEC 62600-101 TS: Marine energy - Wave, tidal and other water current converters - Part 101: Wave energy resource assessment and characterization,* 2014.

[2] "Wave measurement Evaluation and Test : Intercomparison," The Joint WMO-IOC Technical Commission for Oceanography and Marine Meteorology, [Online]. Available: http://www.jcomm.info/index.php?option=com_content&view=article&id=111&Itemid=38.

[3] C. O. Collins III, "In situ wave measurements: sensor comparison and data analysis," University of Miami, 2012.

[4] V. Swail, R. Jensen, J. Turton and et al., "Wave measurement, needs and developments for the next decade," in *OceanObs*, Venice, Italy, 2009.

[5] "Wave measurement Evaluation and Test," The Joint WMO-IOC Technical Commission for Oceanography and Marine Meteorology, [Online]. Available: http://www.jcomm.info/index.php?option=com_content&view=article&id=62.

[6] Nortek, "AWAC with Acoustic Surface Tracking (AST)," Nortek, Providence, RI.

[7] W. Rattanapitikon and T. Shibayama, "Verification and modification of breaker height formulas," *Coastal Engineering Journal,* vol. 4, no. 42, pp. 389-406, 2000.

[8] B. Robertson, H. Bailey, D. Clancy, J. Ortiz and B. Buckham, "Influence of Wave Resource Assessment Methods on Wave Power Production Estimates," in *ICOE*, Halifax, Canada, 2014.

[9] S. J. Beatty, B. J. Buckham and P. Wild, "Modeling , Design and Testing of a Two-Body Heaving Wave Energy Converter," 2007.

[10] B. Robertsob, H. Bailey, D. Clancy, J. Ortiz and B. Buckham, "Influence of Wave Resouce Assessment methods on wave power production estimates," in *International conference on ocean energy*, Nova Scotia, Halifax, 2014.

[11] ProteusDS 2013 Manual. Solver 2.2.1977, Dynamic Systems Analysis Ltd, 2013.

[12] Bailey, H., Ortiz, J., Robertson, B., Buckham, B. and Nicoll, R., "A methodology for wave-to-wire wec simulations," in *Marine Renewable Energy Technology Symposium*, Seattle, WA., 2014.